Regular Article

PHYSICAL CHEMISTRY RESEARCH
Published by the
*Iranian Chemical Society*
www.physchemres.org
info@physchemres.org

*Phys. Chem. Res., Vol. 14, No. 1, 119-140, March 2026*
**DOI: 10.22036/pcr.2025.525982.2687**

# Flavonoids from Algerian Propolis as Potent Antioxidants and ACE2 Receptor Inhibitors: Insights from Molecular Docking, ADME-Tox Prediction, DFT, and Molecular Dynamics

Y. Aimene[a], S. Seridi[a,*], R. Menacer[b, c], A. Braik[a] and A. Seridi[a.]

[a]*Laboratoire de Chimie Physique, Université 8 Mai 1945, BP 401, Guelma 24000, Algeria*

[b]*Centre de Recherche Scientifique et Technique en Analyses Physico-Chimiques CRAPC-Bou-ismaïl, Tipaza, Algeria*

[c]*Pharmaceutical Sciences Research Center -Ali Mendjeli-Constantine- 25000- Algeria*

*(Received 25 May 2025, Accepted 19 November 2025)*

This study aims to explore five flavonoids derived from Algerian propolis, namely phytolarigenin (**L1**), pilosin (**L2**), ladanein (**L3**), chrysin (**L4**), and apigenin (**L5**), using computational tools to assess their antioxidant capacity and ability to inhibit human angiotensin-converting enzyme-2 (ACE2), a key target involved in SARS-CoV-2 entry. DFT calculations were performed to optimize molecular structures, analyze electronic descriptors, and evaluate antioxidant activity *via* HAT, SETPT, and SPLET mechanisms. Among the tested compounds, pilosin (**L2**) exhibited the highest antiradical potency, mainly attributed to its 8-OH group. Molecular docking revealed that all compounds had favorable interactions with the ACE2 active site, with binding scores ranging from -6.31 to -9.67 kcal $mol^{-1}$. Notably, pilosin (**L2**) demonstrated the most stable binding affinity (-9.67 kcal $mol^{-1}$), mainly due to a stable hydrogen bond involving its 8-OH group and $Glu^{375}$ residue. Molecular dynamics simulations confirmed the structural stability of the **L2**/ACE2 complex over 100 ns. Additionally, pharmacokinetic predictions revealed good oral bioavailability and low toxicity for all molecules except **L1**, which showed a positive AMES test. These results strongly highlight pilosin (**L2**) as the leading dual-function candidate with potent antioxidant and antiviral properties, suitable for further drug development efforts.

**Keywords:** Flavonoids, Antiradical activity, ACE2, DFT, Molecular docking and dynamics, ADME-Tox

## INTRODUCTION

In recent years, the coronavirus disease known as COVID-19 has spread rapidly worldwide and raised major public health concerns [1]. This infectious disease is caused by the severe acute respiratory syndrome coronavirus 2 (SARS-CoV-2), which primarily targets the respiratory system, but can also affect the nervous system, kidneys, liver, and gastrointestinal tract [2]. Common symptoms of SARS-CoV-2 infection include headache, muscle pain, shortness of breath, and loss of smell and taste [3,4]. Consequently, there is a pressing need for effective antiviral drugs against COVID-19 [5].

Recent studies show that the SARS-CoV-2 genome is closely related to that of SARS-CoV-1 [6]. Both viruses share a similar cell entry mechanism and bind to the same receptor, angiotensin-converting enzyme 2 (ACE2), to infect host cells [7]. These structural and functional similarities provide a valuable basis for designing potential inhibitors to prevent SARS-CoV-2 infection [8].

ACE2 plays a key role in viral entry by facilitating membrane fusion between the virus and human cells [9]. SARS-CoV-2 binds to the N-terminal helix residues of the ACE2 receptor through its spike glycoprotein [10,11], enabling infection. Therefore, blocking the ACE2 receptor

*Corresponding author. E-mail: seridi.saida@univ-guelma.dz

has emerged as a promising therapeutic approach [12]. Compounds that bind to the ACE2 active site and form stable protein-ligand complexes may prevent viral attachment and entry into host cells [12].

Natural products are promising candidates for antiviral therapies due to their accessibility, low toxicity, and wide range of biological activities [13-15]. Propolis, a resinous substance produced by bees from plant sources, has been used for centuries in traditional medicine [19-21]. It exhibits various bioactivities, including antibacterial, antifungal, antiviral [22], antioxidant, anti-inflammatory [23,24], immunomodulatory, and anticancer effects [25,26]. The chemical composition of propolis varies by geographical origin and botanical source. For example, European propolis is rich in flavonoids and aromatic acids [27], whereas Brazilian propolis contains artepillin C and p-coumaric acid derivatives [28]. These variations may influence its pharmacological potential [29].

Flavonoids are particularly known for their antioxidant properties [30-32]. Recent studies show that flavonoid-rich extracts may inhibit angiotensin-converting enzyme (ACE) activity [33]. Given the structural similarity between ACE and ACE2, ACE inhibitors could potentially block ACE2 as well [34]. Clinical data suggest that hospitalized COVID-19 patients who received ACE inhibitors had better survival outcomes [35]. *In silico* analyses by Güler *et al.* demonstrated that flavonoids from Turkish propolis, such as rutin and quercetin, could bind effectively to the ACE2 receptor [36]. A similar study on Indonesian propolis revealed that isorhamnetin and other flavonoids also showed strong ACE2 binding affinities [37], with docking scores exceeding that of the reference compound MLN-4760.

These encouraging findings highlight the need for further investigation into the antiviral potential of propolis-derived compounds [38]. Algeria, one of the countries affected by COVID-19, harbors a wide variety of propolis types with diverse pharmacological profiles [39-42]. In this study, five flavonoids previously isolated from propolis collected in the Jijel region of northeastern Algeria were selected: pectolinarigenin (**L1**), pilosin (**L2**), ladanein (**L3**), chrysin (**L4**), and apigenin (**L5**), as shown in Fig. 1 [43]. These compounds were structurally identified using NMR and mass spectrometry.

The aim of this work is to assess the antioxidant and ACE2-inhibitory properties of the selected Algerian flavonoids (L1–L5) through computational methods, and to explore the possible correlation between these two properties. Density functional theory (DFT) calculations were used to evaluate antioxidant potential, while molecular docking and dynamics simulations assessed ACE2 binding affinity and complex stability. ADME-Tox properties were also predicted to assess drug-likeness. To the best of our knowledge, this is the first study to associate the antioxidant profile of these flavonoids with their ACE2 inhibitory potential, offering a novel perspective for the development of new anti-COVID-19 therapeutic agents.

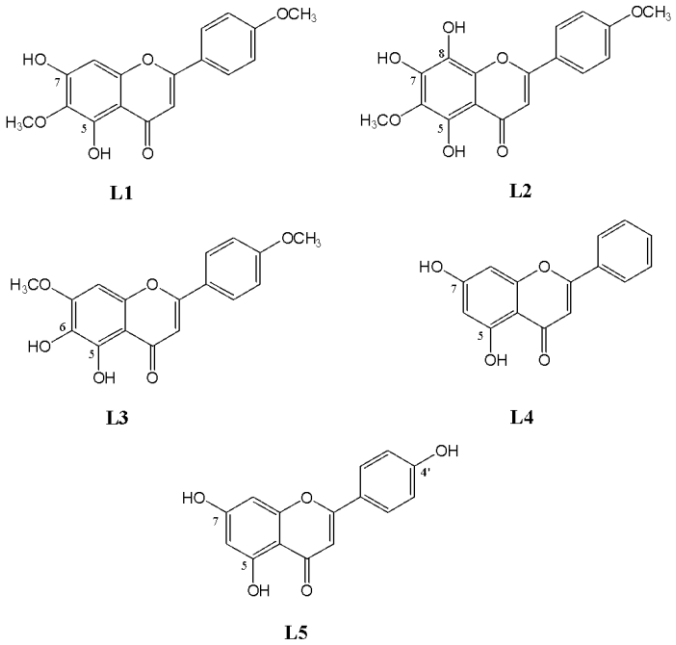


**Fig. 1.** Structures of flavonoids isolated from the Algerian propolis extracts.

## MATERIALS AND METHODS

### DFT Studies

The Gaussian 09 software package [44] was used to perform density functional theory (DFT) calculations for the studied compounds in both gas and aqueous phases**.** Geometry optimizations were carried out using the B3LYP functional with the 6-31G(d,p) basis set [45-48]. Solvent

effects on enthalpies were evaluated using the integral equation formalism polarizable continuum model (IEF-PCM)**.** Energies and enthalpies were computed based on standard statistical thermodynamics formulas and vibrational frequencies obtained at the B3LYP/6-31G(d,p) level, in order to assess the stability of the optimized structures. The B3LYP/6-31G(d,p) level of theory was selected as the most appropriate approach for further calculations, ensuring methodological consistency throughout the analysis [49].

The antioxidant activity of a molecule can be correlated with its chemical structure by using several indices or descriptors, such as Bond Dissociation Enthalpy (BDE), Ionization Potential (IP), Protonic Affinity (PA), Proton Dissociation Enthalpy (PDE), and Electron Transfer Enthalpy (ETE). The type of mechanism gives the choice of the descriptor. Three major mechanisms are described. The first one is the transfer of a hydrogen atom (HAT), associated with BDE measures; the second is the transfer of a single electron followed by a proton (SETPT), estimated by the IP and the PDE; and the third is the loss of a proton followed by an electron (SPLET) evaluated by PA and ETE. By calculating the energy quantities of BDE, IP, PDE, PA and ETE, we can determine the active site (the most reactive OH group) and therefore we can deduce the most probable mechanism for each of the five studied compounds (see Fig. 2) [50]. Using the overall enthalpies of the various species in the gas and water phases, the reaction enthalpy values were calculated as follows:

$$BDE = H(ArO\cdot) + H(H\cdot) - H(ArOH) \quad (1)$$

$$IP = H(ArOH+\cdot) + H(e^-) - H(ArOH) \quad (2)$$

$$PDE = H(ArO\cdot) + H(H^+) - H(ArOH^{+}\cdot) \quad (3)$$

$$PA = H(ArO^-) + H(H^+) - H(ArOH) \quad (4)$$

$$ETE = H(ArO\cdot) + H(e^-) - H(ArO^-) \quad (5)$$

The enthalpies of the hydrogen atom ($H^{\bullet}$), the proton ($H^+$) and the electron ($e^-$) were obtained from previous reports. [51-53,54]. All reaction enthalpies defined in Eqs. (1) to (5) were calculated for an atmospheric pressure of 298.15 K and 1 atm. HOMO and LUMO energies, global reactivity, electronic properties, electrophilicity index and electronegativity descriptors are reported in the second part.

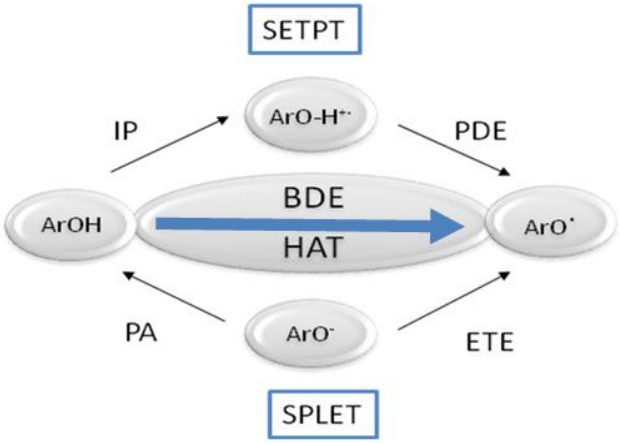


**Fig. 2.** Scheme of the analyzed mechanisms of antioxidant activity.

## Docking Simulation Methods

**Protein preparation.** Two types of ligands were used in molecular docking calculations. The first is the co-crystallized ligand MLN-4760 previously isolated from the ACE2 crystal structure. Redocking of the dipeptide-like inhibitor MLN-4760 in the ACE2 cavity should be an important step in identifying the binding site. The second type, consisting of five flavonoid derivatives extracted from Algerian propolis [43], was designed and optimized as mentioned in the DFT section. 3D coordinates of the ligand structures were converted to pdb file format, and then polar hydrogens, Gasteiger partial charges and rotatable bonds were added using ADTools 1.5.7 [57]. Final prepared molecules were saved in pdbqt files format to be used later as test ligands in the docking simulations, as done in the previous work [59].

**Docking simulation.** Molecular docking involves positioning the test ligand into the enzyme's active site and evaluating various conformations to identify the most favorable binding mode. The AutoDock 4.2 program employs a common approach called semi-rigid docking, *i.e.*, a rigid receptor and flexible ligands [60]. This approach offers advantages such as lower computational cost and faster

screening while preserving ligand flexibility. However, the rigid receptor assumption may overlook conformational changes upon ligand binding and may not fully account for interactions with cofactors. Therefore, docking results should be interpreted with these limitations in mind and further validated by molecular dynamics simulations to capture protein-ligand flexibility [61]. In our study, the ligand's rotatable bonds increased its conformational adaptability within the ACE2 binding site, promoting more favorable interactions with active-site residues. To accelerate energy evaluations, the ACE2 receptor was embedded within a 3D grid box encompassing the active site, allowing free ligand rotation. Using the AutoGrid subprogram [57], the grid center was set at coordinates X = 40.199, Y = 6.144, Z = 29.006, with dimensions 45 × 45 × 45 Å$^3$. Docking calculations were performed using the Lamarckian Genetic Algorithm (LGA) implemented in AutoDock 4.2 [57] with 100 independent runs and an RMSD tolerance of 2.0 Å. All other parameters were retained at their default values [57].

**Validation of the docking protocol.** To check the validity of the docking protocol described above, the native inhibitor MLN-4760 was redocked. The redocking process is a method in which the inhibitor MLN-4760 is docked back in its original position inside the ACE2 cavity. The protocol is considered valid if the docked free energy is negative and the RMS deviation between the X-ray structure and the predicted conformation of inhibitor MLN-4760 is less than 2.0 Å [62]. After validating the docking method, this protocol can be applied to dock our flavonoid compounds inside the ACE2 receptor in the same area occupied by the native ligand MLN-4760.

**Molecular dynamics.** The best docking pose, *i.e*., pilosin/ACE2, was used in molecular dynamics (MD) computations to gain insight into the protein-ligand interaction stability. The CHARMM-GUI solution builder was used to create the input files using the CHARMM force field [63,64]. The ligands' topology was developed by CHARMM General Force Field using the Param-Chem server [64]. The periodic boundary conditions (PBC) were defined then the system's energy was minimized. The complex was then subjected to an NVT and an NPT ensemble to equilibrate the complex for stabilizing its temperature and pressure. Finally, the complex is subjected to a production simulation run for 100 ns in NPT ensemble at 300.15 K and 1 bar. The trajectories were stored every 2 ps. Simulations of 100 ns in NPT assembly were performed for the production stage. The LINCS algorithm was used for constraining H-bonds GROMACS 2020.2 software [65] was used for all MD calculations, applying the CHARMM36 force field. Protein-ligand interaction frequency analysis and trajectory visualization were both performed using the VMD molecular graphics tool [66].

**ADME-Tox and physicochemical properties.** In order to predict the bioactivity of selected flavonoids in the human body, we need to determine the drug-likeness and pharmacokinetic properties. For this purpose, we exploited the pkCSM webserver [67] (https://biosig.lab.uq.edu.au/pkcsm/prediction) to calculate the ADME-Tox parameters (absorption, distribution, metabolism, excretion and toxicity). Furthermore, the SwissADME server (http://www.swissadme.ch) was applied for analyzing druglike properties [68].

## RESULTS AND DISCUSSION

### DFT Calculations

This computational study aims to explore more details about the structural properties of the flavonoid compounds and whether there is any effect on biological activity.

**The H atom transfer (HAT) bond dissociation enthalpies.** The aryloxyl radical ($^{ArO^{\bullet}}$) can be formed directly by phenolic hydrogen transfer towards a radical of high energy, such as the degradation of fatty acids, which can give organic radicals ($R^{\bullet}$). These reactions, of H atom transfer and/or electrons with the conversion of a highly reactive radical to a resonance-stabilized aryloxyl radical, are one of the main mechanisms of antioxidant actions of phenols. Thus, the homolytic dissociation energy of the O-H bond can be used to measure phenol's capacity to produce an H atom (energy dissociation bond, BDE). The O-H bond breaks more easily, thus antioxidant reactivity increases with decreasing BDE levels. Table 1 summarizes the computed findings in gas and water. Based on the BDE values given in Table 1, the hydrogen-donating strength of flavonoids in the water and gas phase was in the following order: **L2 > L3 > L5 > L1 > L4**. As shown in table 1, the 8-OH BDE of compound **L2** is the lowest compared to the other OH groups in the gas phase and water, at 73.49 and 71.35 kcal mol$^{-1}$,

respectively. This indicates that H atom transfer from the 8-OH of compound **L2** is easier than from other OH groups, and the homolytic cleavage of 8-OH most likely occurs to transfer the H atom to the free radical. Therefore, 8-OH of compound **L2** plays a critical role in the HAT antioxidative mechanism. On the other hand, the O-H bond dissociation enthalpies in the water and gas phases are not significantly different from one another; for example, the largest deviation between the BDE in the gas phase and that in water is 5.24 kcal $mol^{-1}$. These results support the undermentioned docking studies, in which 8-OH interactions of pilosin (**L2**) play an essential role in maintaining the Receptor-Ligand system's stability.

**Electron transfer-Proton transfer (SETPT).** Ionisation Potential: A two-step mechanism in which an electron is transferred from a flavonoid to a free radical in the first step and a proton is transferred in the second (reaction 6).

$$ArOH + ROO^{\bullet} \rightarrow ArOH^{+\bullet} + ROO^{-} \rightarrow ArO^{\bullet} + ROOH \qquad (6)$$

This mechanism is governed by the electron transfer capacity, that is, the ionization potential (IP). The IP of a molecule is the minimum energy required to remove an electron. The more an aromatic compound is substituted by electron donor groups, the lower its IP and the greater its reducing character. The second step in this reaction is the dissociation of the heterolytic O-H bond. The radical-cation formed is a strong acid that immediately deprotonates and leads to a phenoxyl or aryl radical. To estimate the contribution of the SETPT mechanism of the compounds, we calculated the IP for all flavonoids. The calculated IP values of the investigated compounds, both in the gas phase and in water, have been presented in Table 2. According to the results given in Table 2, it is observed that the sequence of IP values in the gas phase is: **L2 < L3 < L1 < L5 < L4**; whereas the tendency of IP values in water is quite different (**L1 < L2 < L3 < L5 < L4**). This indicates that the radicals are charged and quite sensitive to solvent polarity. However, the formation of neutral species is unfavorable in an aqueous solution [54].

Proton dissociation enthalpies: The next step of the mechanism SETPT is proton transfer, which is described by the proton dissociation enthalpy (PDE). Table 1 details the calculated PDE values in the gas phase and water with various -OH substitutions for all flavonoids. In the case of compounds **L1** and **L4**, the hydroxyl group at position 7 (7-OH) of the aromatic ring had the lowest gas O-H PDE value of 249.63 kcal $mol^{-1}$ and 229.81 kcal $mol^{-1}$,

**Table 1.** Computed Values of BDE (kcal $mol^{-1}$), PA (kcal $mol^{-1}$), ETE (kcal $mol^{-1}$) and PDE (kcal $mol^{-1}$) at 298.15 K and 1 atm, Using the B3LYP/6-31G(d,p) Method

| Compounds | | BDE (O-H) | | ΔBDE[a] | PA | | ΔPA[b] | ETE | | ΔETE[c] | PDE | | ΔPDE[d] |
|---|---|---|---|---|---|---|---|---|---|---|---|---|---|
| | | Gas | Water | | Gas | Water | | Gas | Water | | Gas | Water | |
| **L1** | 5-OH | 92.58 | 87.89 | -4.69 | 357.64 | 68.48 | -289.19 | **50.93** | **95.46** | 44.53 | 256.45 | 141.23 | -115.22 |
| | 7-OH | **85.7**7 | **84.06** | -1.71 | **344.68** | **59.27** | -285.41 | 57.07 | 100.84 | 43.77 | **249.63** | **137.40** | -112.23 |
| **L2** | 5-OH | 88.19 | 83.47 | -4.72 | 359.51 | 69.64 | -289.87 | 44.64 | 89.87 | 45.23 | 403.41 | 136.81 | -266.60 |
| | 7-OH | 77.03 | 75.45 | 1.58 | 336.05 | **53.30** | -283.75 | 56.97 | 98.20 | 41.23 | 392.27 | 128.79 | -263.48 |
| | 8-OH | **73.49** | **71.35** | -2.14 | **351.46** | 63.74 | -287.72 | **38.01** | **86.26** | 48.25 | **385.76** | **124.69** | -261.07 |
| **L3** | 5-OH | 86.30 | 81.92 | -4.38 | **353.90** | 64.78 | -289.12 | 48.38 | 93.19 | 44.81 | 253.16 | 135.26 | -117.9 |
| | 6-OH | **77.15** | **73.39** | -3.76 | 356.59 | **66.44** | -290.15 | **36.54** | **83.00** | 46.46 | **244.01** | **126.73** | -117.28 |
| **L4** | 5-OH | 99.16 | 94.00 | -5.16 | 359.41 | 69.51 | -289.9 | **55.73** | **100.53** | 44.8 | 242.51 | 11.82 | -230.69 |
| | 7-OH | **86.47** | **86.61** | 0.14 | **340.36** | **57.17** | -283.37 | 62.09 | 105.48 | 43.39 | **229.81** | **4.43** | -225.38 |
| **L5** | 5-OH | 99.31 | 94.07 | -5.24 | 360.54 | 70.19 | -290.35 | **54.74** | 101.92 | 47.18 | 246.91 | 14.22 | -232.69 |
| | 7-OH | 86.09 | 86.17 | 0.08 | 341.34 | 57.67 | -283.67 | 60.74 | 104.54 | 43.8 | 233.69 | 6.32 | -227.37 |
| | 4'-OH | **81.60** | **82.16** | 0.56 | **333.30** | **56.82** | -276.48 | 64.25 | **101.38** | 37.13 | **229.19** | **2.30** | -226.89 |

All values are in kcal $mol^{-1}$. [a]ΔBDE = ΔBDE (water) – ΔBDE (gas). [b]ΔPA = PA (water) – PA (gas). [c] ΔETE = ETE (water) – ETE (gas). [d]ΔPDE = PDE (water) − PDE (gas). *The lowest values are in bold.

respectively. On the contrary, the gas O-H PDE values of hydroxyl groups 8-OH (385.76 kcal $mol^{-1}$) and 6-OH (244.01 kcal $mol^{-1}$) of the compounds **L2** and **L3**, respectively, were lower than that obtained at other -OH positions. In addition, the lowest PDE value was obtained at position 4′ of the aromatic ring for compound **L5** with 229.19 kcal $mol^{-1}$. PDE in water has significantly lower values than the values corresponding to the gas phase [54].

**Table 2.** Ionisation Potential at 298.15 K of Five Flavonoids Using the B3LYP/6-31G(d,p) Method

| Compounds | IP (kcal $mol^{-1}$) | |
|---|---|---|
| | Gas | Water |
| **L1** | 152.06 | 78.30 |
| **L2** | 146.24 | 116.69 |
| **L3** | 149.06 | 124.86 |
| **L4** | 172.64 | 136.26 |
| **L5** | 168.38 | 133.94 |

**The sequential proton loss electron transfer (SPLET).** The SPLET mechanism represents an inhomogeneous dissociation reaction mainly characterized by two thermodynamic parameters, proton affinity (PA, reaction 4) and electron transfer enthalpy (ETE, reaction 5). Table 1 shows that the gas-phase proton affinity PA values were considerably higher than those of BDEs for all studied flavonoids. However, all PA values calculated in water were lower than the obtained BDE values. Also, the results in Table 1 showed that the aqueous solvent significantly affects the PA and PDE values; the variation between PA in the gas phase and aqueous solution ranges from -276.48 to -290.35 kcal $mol^{-1}$. These results indicate that the SPLET mechanism prefers the aqueous solvent from a thermodynamic point of view.

The ETE values are always lower than the IP values in the gas phase and water. This indicates that the anionic form's unique electron transfer process is preferable to that of the neutral form, which is consistent with the results obtained in other studies [69-71]. From the ΔETE values, which are presented in Table 1, it can be noted that the solvation effect of the water induces an increase in the ETE. As a result, the solvent in the water is unfavorable for the following electron transfer process.

As a conclusion, on the one hand, the calculated BDE, IE+PDE and PA+ETE of OH groups in the gas phase and in water show the following same orders: **L1**: 7-OH < 5-OH, **L2**: 8-OH < 7-OH < 5-OH, **L3**: 6-OH < 5-OH, **L4**: 7-OH < 5-OH and **L5**: 4'-OH < 7-OH < 5-OH. Consequently, O7, O8, O6, O7, and O4' are the positions exhibiting the lowest energies and the strongest antiradical power. In addition, the antiradical potency of the studied flavonoids ranks as follows: **L2** > **L3** > **L5** > **L1** > **L4**. Interestingly, this is the same for HAT, SPLET, and SET-PT. On the other hand and regarding the first steps of the three studied mechanisms (Table 1), the antiradical mechanisms show the following favored trend: HAT > SET-PT > SPLET in the gas phase and SPLET > HAT > SET-PT for water, expect for L1, which exhibits the following favored trend: SPLET > SET-PT > HAT.

## HOMO–LUMO Calculations for Flavonoids

Molecular orbitals can help to elucidate molecules' reactivity, structural and physical characteristics. The two most influential orbitals in a molecule, *i.e.*, the highest occupied molecular orbital (HOMO) and the lowest unoccupied molecular orbital (LUMO), otherwise known as frontier molecular orbitals (FMO), play a key role in defining various properties [72]. These include the energy gap between the HOMO and LUMO, which decides the hardness, kinetic stability and chemical reactivity [73]. According to Janak's theorem, IP and EA are roughly related to the energies of the HOMO and LUMO orbitals [73,74].

The HOMO and LUMO of all flavonoids were obtained using the DFT method at B3LYP/6-31G(d,p) and then visualized in Fig. 3. The energies of HOMO and LUMO for the five flavonoids are given in Table 3. The $E_{LUMO}$ values have a low magnitude, which could indicate the soft electrophile behavior of flavonoids [75]. Higher values of $E_{HOMO}$ could indicate better electron-donating ability and antioxidant activity of flavonoids.

The energy gap for all test compounds was between 3.66 eV and 4.16 eV, while pilosin (**L2)** has the smallest gap, making it the most reactive. This is consistent with the solid ligand-receptor affinity (ΔG = -9.67 kcal $mol^{-1}$) recorded between **L2** and the ACE2 receptor (see molecular docking section).

**Table 3.** Ionisation Enthalpy and Electron Affinity Global Reactivity Descriptors Calculated for the Five Flavonoids through the Orbital Vertical Method

| Compounds | LUMO (eV) | HOMO (eV) | Gap* (eV) | IP (eV) | EA (eV) | η | χ | μ | ω | S |
|---|---|---|---|---|---|---|---|---|---|---|
| **L1** | - 1.70 | -5.78 | 4.08 | 5.78 | 1.70 | 2.04 | 3.74 | -3.74 | 3.42 | 0.24 |
| **L2** | -1.66 | -5.32 | 3.66 | 5.32 | 1.66 | 1.83 | 3.49 | -3.49 | 3.32 | 0.27 |
| **L3** | -1.68 | -5.39 | 3.71 | 5.39 | 1.68 | 1.85 | 3.53 | -3.53 | 3.36 | 0.27 |
| **L4** | -1.88 | -6.00 | 4.12 | 6.00 | 1.88 | 2.06 | 3.94 | -3.94 | 3.76 | 0.24 |
| **L5** | -1.74 | -5.90 | 4.16 | 5.90 | 1.74 | 2.08 | 3.82 | -3.82 | 3.50 | 0.24 |
| QUERCETIN [75] | | | | | | 1.69 | 4.00 | -4.00 | 4.72 | 0.29 |
| ALPINETIN [80] | | | | | | 2.45 | 3.90 | -3.90 | 3.09 | 0.20 |

(*) Gap = $E_{LUMO}$-$E_{HOMO}$ (absolute value).

Electronic properties were calculated based on the values of ionisation energy and electron affinity. Additional chemical descriptors such as electronegativity (χ), electrophilicity (ω) [76], softness (S), hardness (η), and chemical potential (μ) can be determined employing the equations given below [77-79]:

$$Electronegativity\ (\chi) = \frac{IP+EA}{2} \quad (7)$$

$$Electrophilicity\ index\ (\omega) = \frac{\mu^2}{2\eta} \quad (8)$$

$$Softness\ (S) = \frac{1}{2\eta} \quad (9)$$

$$Hardness\ (\eta) = \frac{IP-EA}{2} \quad (10)$$

$$Chemical\ potential\ (\mu) = \quad - \chi \quad (11)$$

The computed chemical descriptor values of flavonoids are listed in Table 3. The ionization potential is the energy required to extract an electron from a molecule. In contrast, the energy emitted from adding an electron to a neutral molecule is known as electron affinity. Calculated ionization potential (IP) values for flavonoids were around 5.32 eV to 6 eV, while electron affinity (EA) was between 1.66 eV and 1.88 eV. These values show that flavonoids tend to release electrons. The values reached here are consistent with the ionisation and electron affinity values for Quercetin [75] (IP = 5.69 eV; EA = 2.31 eV) and Alpinetin [80] (IP = 6.35 eV; EA = 1.44 eV).

Electroegativity and electrophilicity index measure both the tendency to attract the electron pair and the electron affinity, respectively. The hardness descriptor reflects the resistance to charge transfer, and the contrary of hardness is another descriptor known as softness [81]. Electronegativity and electrophilicity index follows the order **L2** < **L3** < **L1** < **L5** < **L4**, whereas hardness follows the order **L2** < **L3** < **L1** < **L4** < **L5**. These descriptors for flavonoids were tabulated in Table 3. These descriptors had values comparable to Quercetin [75] and Alpinetin [80], which are potent antioxidant molecules. According to Table 3, all the values associated with the chemical potential turn out low; thus, these flavonoids will tend to release electrons rather than accept them. This is quite favorable for antioxidant activity.

## Molecular Docking

**Virtual screening analysis.** Molecular docking computations were performed to assess the potential interactions of five flavonoid derivatives (**L1** to **L5**) with the human ACE2 protein. The AutoDock 4.2 software, used for this end, employed the semi-rigid approach that facilitates the search for favorable conformations and minimizes the error margin [82]. The docked free energy (ΔG) between the target protein ACE2 and the native inhibitor MLN-4760 was determined to evaluate the potency and accuracy of the AutoDock 4.2 program in reproducing the correct binding mode of the co-crystal structure (pdb id: 1R4L). A negative docking score means the ligand is effectively bound to the protein [83,84]. Contrariwise, a positive energy value signifies that the protein-ligand complex has not formed, meaning that the docking protein-ligand system has not indicated a bond [85]. As shown in Table 4, the inhibitor MLN-4760 has a docking score of -10.27 kcal $mol^{-1}$.

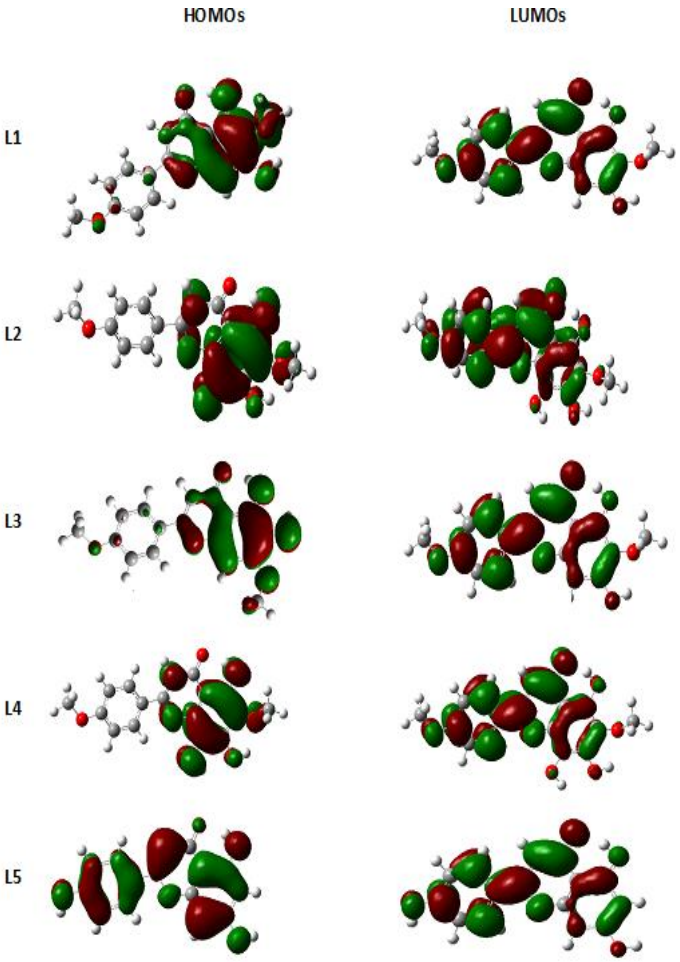


**Fig. 3.** Frontier molecular orbital pictures of the five flavonoids calculated using DFT.

This energy value differs from that of Terali's team [86], possibly due to the changes in the docking program and parameters employed. In contrast, an RMSD value of 0.75 Å (below 2.0 Å) indicates that the small molecule MLN-4760 binds in the same zone as before without changing its conformation to fit into the bore. The RMSD value was strongly supported by visual analysis, as presented in Fig. 4, which showed great alignment between the re-docked conformation and the native geometry (given by X-ray diffraction) of the MLN-4760 inhibitor.

Besides, to confirm the accuracy of the docking tool parameters, the protein-ligand binding mode generated by the AutoDock 4.2 program was analyzed and compared to that found in the crystallographer's paper. Generally, the binding profile obtained by molecular docking for the re-docked inhibitor resembles that found in the co-crystallized structure MLN-4760. Details of the interaction profile were discussed in the next section of the interaction mode analysis. From these preliminary findings, the docking method is considered reasonably acceptable to predict correct enzyme-inhibitor interactions and can be used for virtual screening.

Likewise, we docked five flavonoid ligands (not available in the PDB) in the binding cavity occupied by the natural ligand using the ACE2 model (PDB code: 1R4L) with the same parameters. Given the obtained results, the best poses for all the flavonoids were well placed in the ACE2 binding site, where they are aligned with the natural inhibitor MLN-4760 (see Fig. 5). Moreover, Table 4 presents negative scores for all test flavonoids, ranging from -6.31 to -9.67 kcal $mol^{-1}$. Among five flavonoids, we found that the compound **L2** has the lowest binding energy of -9.67 kcal $mol^{-1}$ (see Table 4). A lower value of the docking score (ΔG) indicates higher ligand-receptor affinity [83]. Accordingly, the pilosin-ACE2 complex should be more stable and requires further investigation.

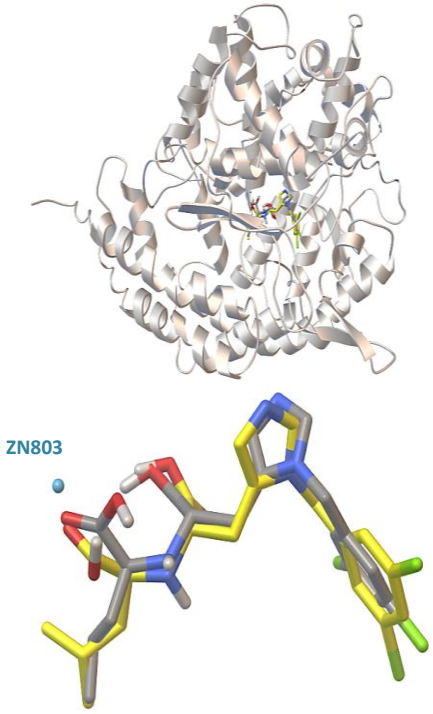


**Fig. 4.** Superposition of the geometries of the natural (yellow carbon) and re-docked (gray carbon) ligand MLN-4760 in the active site of ACE2, showing strong structural overlap.

**Table 4.** Docking Scores of the Interaction of the Natural Inhibitor and Test Flavonoids with the ACE2 Receptor

| Compounds | ΔG (Kcal $mol^{-1}$) | Distance of Zn-O interaction (Å) | Number of interactions | H-bonds number | Binding similarity |
|---|---|---|---|---|---|
| ***MLN-4760** | -10.27 | 1.84 | 28 | 8 | 100% |
| **L1** | -7.20 | 1.88 | 20 | 3 | 66% |
| **L2** | -9.67 | 1.75 | 23 | 5 | 78% |
| **L3** | -7.16 | 1.98 | 22 | 3 | 44% |
| **L4** | -6.31 | 1.68 | 17 | 1 | 46% |
| **L5** | -6.53 | 1.88 | 16 | 1 | 42% |

*Natural ligand as a control.

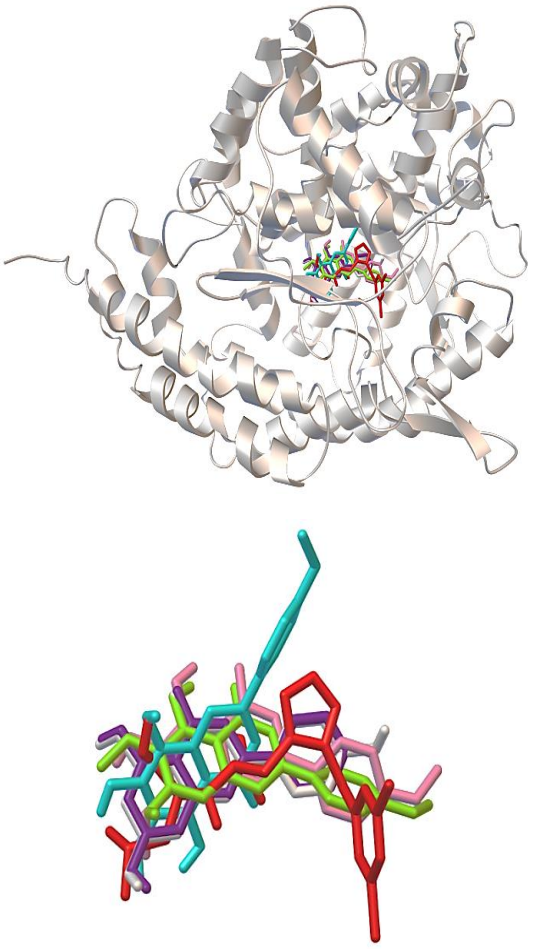

**Fig. 5.** Alignment of the flavonoid ligands with the native inhibitor MLN-4760 in the ACE2 active site. Color codes: MLN-4760 in red, **L1** in green, **L2** in azure**, L3** in pink, **L4** in purple, and **L5** in white. All flavonoids maintain close contact with $Zn^{2+}$, with Zn–O distances ranging from 1.68 to 1.98 Å.

## Interaction Mode Analysis

To understand the mechanism of ACE2 inhibition, we examined its crystal structure in native (open) and inhibitor-bound (closed) forms. The extracellular domain of ACE2 consists of two subdomains separated by an active-site cleft [55]. Subdomain 1 contains the zinc catalytic site and N-terminus (residues 19-102, 290-397, and 417-430), and mediates hydrogen and ionic interactions with the SARS-CoV-2 Spike RBD [7]. Subdomain 2 includes the C-terminus (residues 103-289, 398-416, and 431-615) [55]. Binding of MLN-4760 to the ACE2 cleft induces closure of the two subdomains around the inhibitor, displacing key spike-binding residues by 6-9 Å [55], thereby hindering viral attachment.

In this study, MLN-4760 was redocked into the ACE2 cleft using AutoDock 4.2 software. Binding interactions at the zinc-containing site were analyzed and visualized using Biovia Discovery Studio. According to Fig. 6, the terminal carboxylate group of the redocked inhibitor MLN-4760 was found to bind the zinc atom through the carbonyl oxygen atom. Notably, the most common drugs targeting zinc-dependent metalloenzymes incorporate phosphonate, phosphate, hydroxamate, carboxylate and sulfonamide functional groups [87,88]. These functionalities, known as zinc-binding groups (ZBGs), are recognized for their ability to coordinate at the catalytic site (*via* a $Zn^{2+}$ ion) through a heteroatom (O, N, or S), thereby substituting for the coordinated water molecule [87]. In addition, several non-covalent interactions were observed between MLN-4760 and

the ACE2 active site cleft, such as electrostatic, hydrophobic, van der Waals and hydrogen bonds. Hydrogen bonding is considered the most influential among weak interactions in determining binding energy [89]. Essential amino acids involved in hydrogen interactions with MLN-4760 are $Arg^{273}$, $His^{345}$, $Pro^{346}$, $Glu^{375}$, $His^{505}$, and $Tyr^{515}$ (see Table 5 and Fig. 6); they are critical for identifying the ACE2 active site [55]. As explained by Guy et al. [90], $His^{345}$ plays a central role in ACE2 inhibition by acting as a hydrogen bond donor or acceptor during host–guest complex formation, while $Glu^{375}$ stabilizes hydrogen-donating groups (*e.g.*, -OH or -NH units) and helps orient the ligand within the binding pocket. Known inhibitors such as MLN-4760 commonly exploit these interactions [55]. Herein, $Glu^{375}$ formed two hydrogen bonds with MLN-4760, one *via* its carboxyl oxygen and the inhibitor's secondary amine, and another with the ZBG hydroxyl group, at distances of 2.36 Å and 1.90 Å, respectively (see Table 5 and Fig. 6). The second carboxylate group of MLN-4760 interacted with $Arg^{273}$, $His^{345}$, $His^{505}$ and $Tyr^{515}$. Moreover, the carbonyl oxygen of $Pro^{346}$ was within H-bonding distance (1.87 Å) of the inhibitor's secondary amine. These interactions closely resemble those of X-ray diffraction [55]. However, crystallographic data indicate a hydrogen bond between the $Tyr^{515}$ phenolic group and the ZBG of MLN-4760, as well as another between $Thr^{371}$ and its imidazole ring. The exclusion of non-protein molecules may account for slight variations in these interactions [55].

In light of the interaction profile established for MLN-4760, we extended our analysis to explore the binding modes of selected flavonoids within the ACE2 active site. Using the hydrogen-bonding residues involved in MLN-4760 binding as reference targets, the test ligands displayed comparable interaction patterns, with similarity scores ranging from 42% to 78% (Table 4). This is evidenced by interactions with key catalytic residues, $Arg^{273}$, $His^{345}$, $Pro^{346}$, $Glu^{375}$ and $His^{505}$ [90]. As illustrated in Fig. 7, $His^{505}$ and $His^{345}$ formed the highest interaction frequencies across all docked flavonoids, followed by $Arg^{273}$ and $Glu^{375}$. As well, the zinc-coordinated residues, $His^{374}$, $His^{378}$, and $Glu^{402}$, were engaged in hydrophobic, electrostatic and van der Waals contacts.

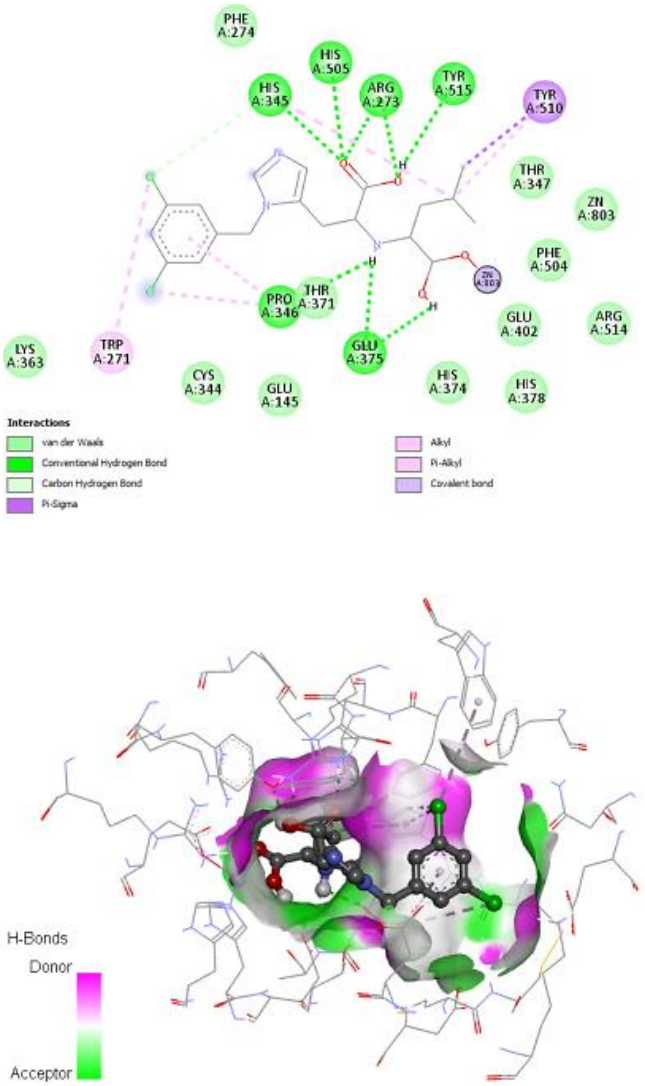


**Fig. 6.** 2D (left) and 3D (right) representations of the ACE2 active site showing side amino acids involved in various contacts with the re-docked inhibitor MLN-4760. Key hydrogen bonds are formed with $Arg^{273}$ (2.09 Å, 2.13 Å), $His^{345}$ (1.87 Å), $Pro^{346}$ (2.65 Å), $Glu^{375}$ (2.36 Å, 1.90 Å), $His^{505}$ (206 Å) and $Tyr^{515}$ (2.09 Å). $Zn^{2+}$ coordination was maintained via the carboxyl group (1.84 Å).

**Table 5.** Hydrogen Bond Distances between the Reference and Test Ligands and ACE2 Active Site Residues

| 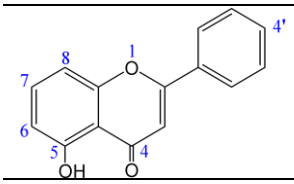 | H-bonds distance (Å) | Residues | | Ligands | Type |
|---|---|---|---|---|---|
| | | Interacting Residues | Binding group | Binding group | A: Acceptor D: Donor |
| ***MLN-4760** | 2.09 | $Arg^{273}$ | $-NH_2$ | =O | D•••A |
| | 2.13 | | $-NH_2$ | −OH | D•••A |
| | 1.87 | $His^{345}$ | −NH | =O | D•••A |
| | 2.65 | $Pro^{346}$ | =O | −NH | A•••D |
| | 2.36 | $Glu^{375}$ | =O | −NH | A•••D |
| | 1.90 | | =O | −OH | A•••D |
| | 2.06 | $His^{505}$ | −NH | =O | D•••A |
| | 2.09 | $Tyr^{515}$ | −OH | −OH | A•••D |
| **L1** | 2.09 | $His^{345}$ | −NH | 1−O | D•••A |
| | 1.99 | $Pro^{346}$ | =O | 7−OH | A•••D |
| | 2.98 | $Arg^{518}$ | $-NH_2$ | 4=O | D•••A |
| **L2** | 1.99 | $Arg^{273}$ | $-NH_2$ | 4=O | D•••A |
| | 1.72 | $His^{345}$ | −NH | 4=O | D•••A |
| | 2.04 | | −NH | 5−OH | D•••A |
| | 1.81 | $Glu^{375}$ | −O | 8−OH | A•••D |
| | 1.82 | $His^{505}$ | −NH | 4=O | D•••A |
| **L3** | 2.01 | $His^{345}$ | −NH | I−O | D•••A |
| | 2.88 | $His^{505}$ | −NH | 1−O | D•••A |
| | 2.39 | $Arg^{518}$ | $-NH_2$ | 4=O | D•••A |
| **L4** | 1.79 | $His^{345}$ | −NH | I−O | D•••A |
| **L5** | 1.73 | $His^{345}$ | −NH | I−O | D•••A |

*Natural ligand as a control.

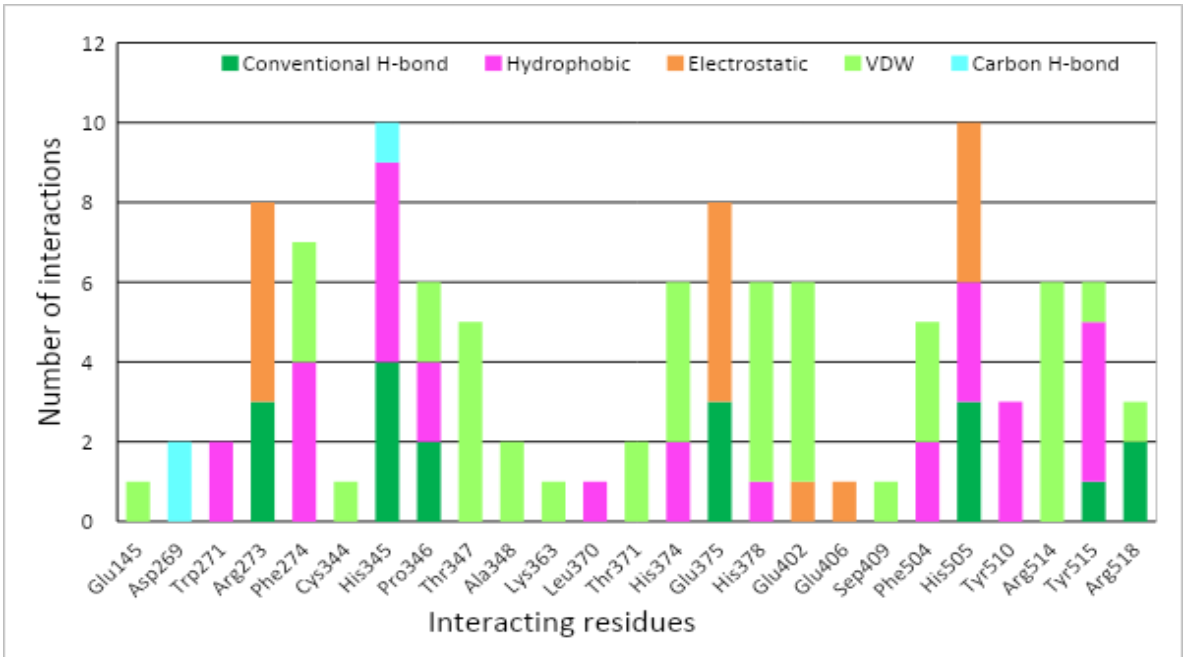


**Fig. 7.** Histogram showing the frequency of interaction of flavonoid ligands with ACE2 catalytic residues. $His^{345}$ and $His^{505}$ displayed the highest contact frequency, followed by $Arg^{273}$ and $Glu^{375}$.

Moreover, as shown in Figs. 8 and 9, all flavonoid ligands were monodentate coordinated to the zinc cofactor via hydroxyl groups on their aromatic rings. Specifically, the zinc-binding hydroxyl group was located at position 5-OH in **L1**, **L3**, **L4**, and **L5**, and at position 8-OH in **L2**. The distance between the $Zn^{2+}$ ion and the nearest ZBG oxygen atom ranged from 1.68 Å to 1.98 Å for all ligands (see Table 4). These short distances reflect the strong ZBG coordination to the ACE2 metal center [87].

Additionally, the docking results revealed five hydrogen bonds for **L2**, three for each of **L1** and **L3**, and only one for **L4** and **L5**. In particular, **L2** demonstrated the most favorable interaction profile, with the lowest binding energy (-9.67 kcal $mol^{-1}$) and the highest binding mode similarity (78%). This can be attributed to its additional aromatic -OH groups, which increase its capacity to form multiple hydrogen bonds compared to the other flavonoid derivatives. As shown in Table 5, three amino acids, $Arg^{273}$, $His^{345}$ and $His^{505}$ were H-bonded to the 4-OH group of **L2** with distances of 1.99 Å, 1.72 Å and 1.82 Å, respectively. $His^{345}$ also formed a hydrogen bond from its imidazole group to the adjacent **L2** 5-OH, with a distance of 2.04 Å. The zinc-bound 8-OH group of **L2** exhibited a favorable H-bond distance of 1.81 Å with $Glu^{375}$. Remarkably, these hydrogen bond distances were shorter, and thus potentially stronger, than those observed for the native inhibitor MLN-4760. **L2** also formed multiple π-anion, π-π, π-alkyl, and van der Waals interactions with vital residues (Fig. 8). Such stable interactions underscore the inhibitory potential of pilosin (**L2**). This behavior was further supported by its electronic properties, including a narrow HOMO–LUMO gap (3.66 eV) and a low 8-OH BDE (73.49 kcal $mol^{-1}$ in gas, 71.35 in water), which favor charge transfer and hydrogen donation within the protein active site [91-93].

In recent studies, Dey *et al.* [94] reported high ACE2 affinity for flavonoids such as Flemiflavanone D and Rhamnetin (-10.2 and -9.1 kcal $mol^{-1}$, respectively), while Obakachi *et al.* [95] highlighted stable binding of xanthone derivatives (XAN71, XAN72) to vital residues such as $Arg^{273}$, $Glu^{375}$, and $His^{345}$. Pilosin (**L2**) displayed comparable binding strength and advantageous electronic characteristics.

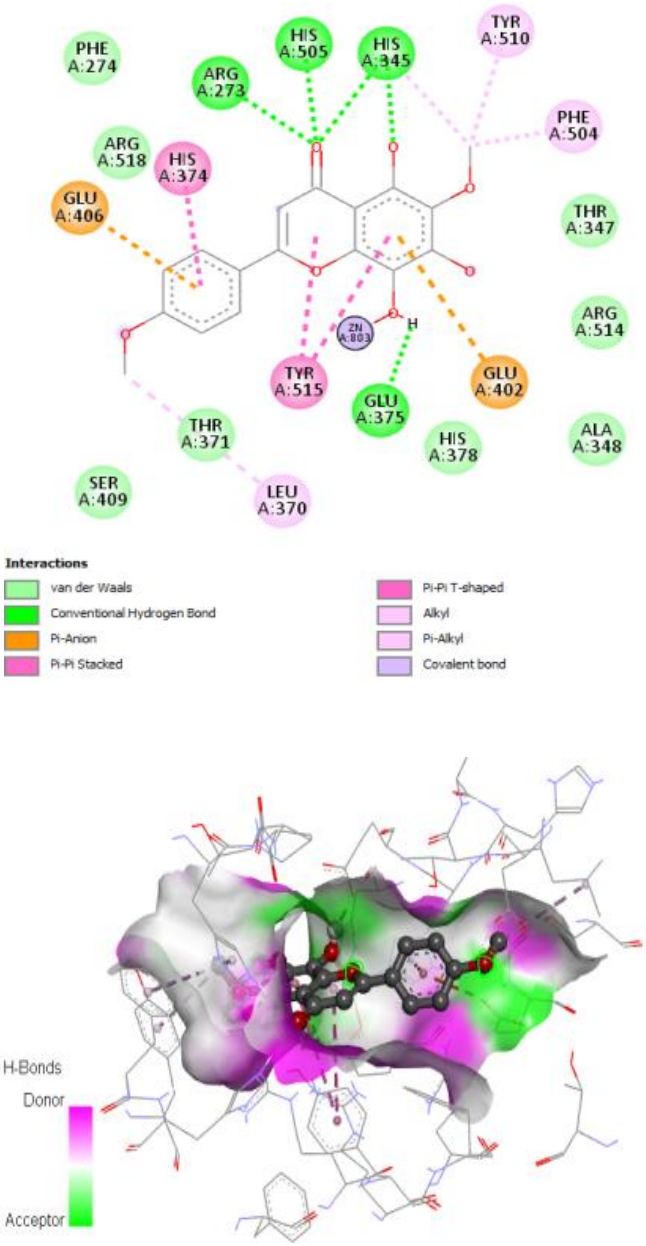


**Fig. 8.** 2D (left) and 3D (right) binding profiles of **L2** with ACE2 cavity. 8-OH and 5-OH groups formed H-bonds with $Glu^{375}$ (1.81 Å) and $His^{345}$ (2.04 Å), respectively, while the 4=O group H-bond interacted with $Arg^{273}$ (1.99 Å), $His^{345}$ (1.72 Å), and $His^{505}$ (1.82 Å). Coordination with $Zn^{2+}$ occurs *via* the 8-OH group (1.75 Å).

**L1**

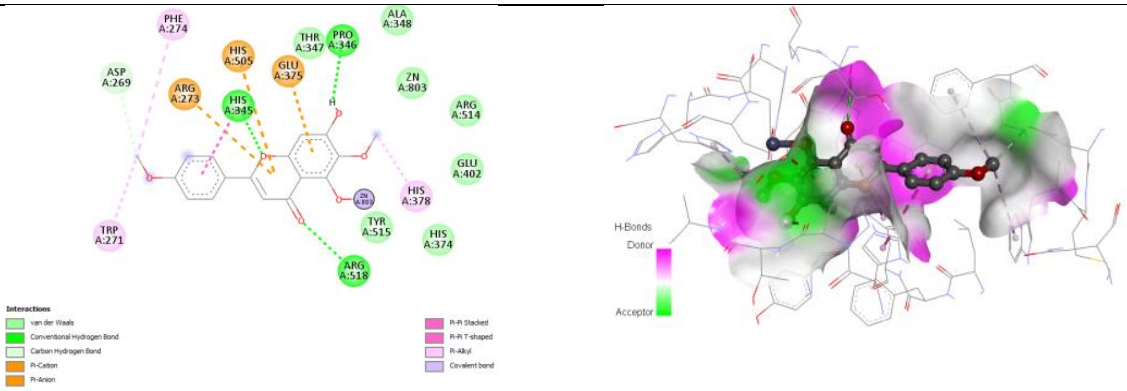


**L3**

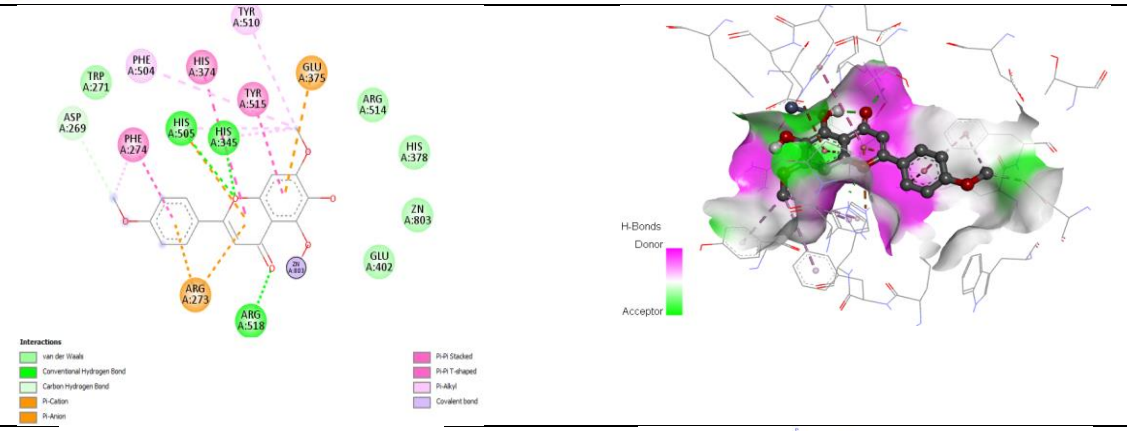


**L4**

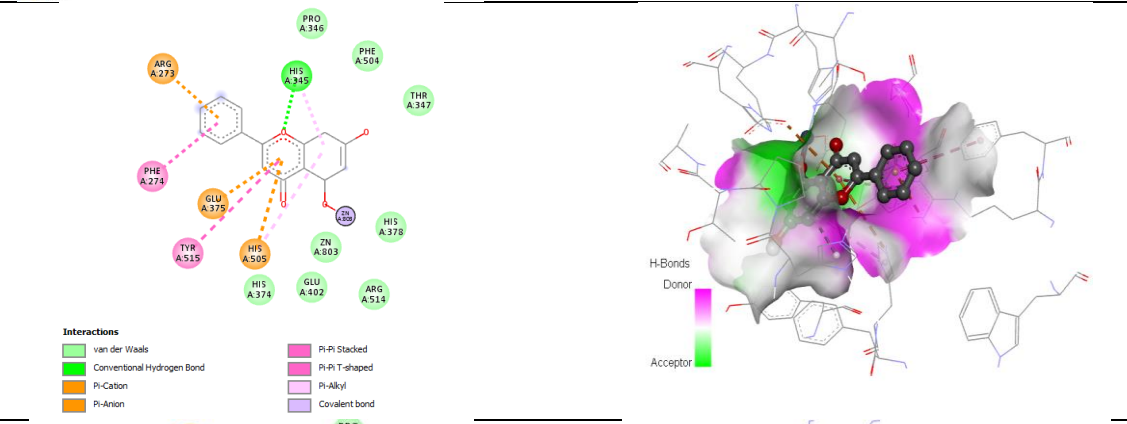


**L5**

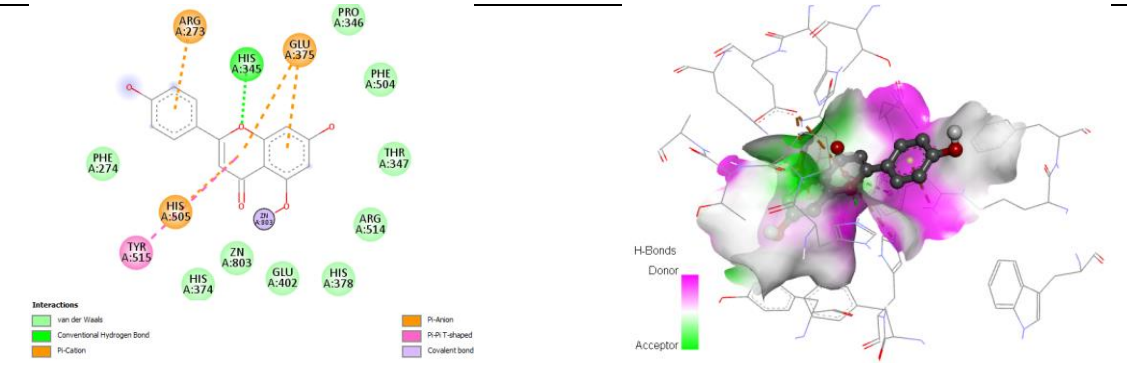


**Fig. 9.** 2D (left) and 3D (right) interactions of flavonoids **L1**, **L3**, **L4**, and **L5** with the ACE2 active site. All ligands coordinate with $Zn^{2+}$ *via* their 5-OH groups (1.68-1.98 Å). **L1** and **L3** form hydrogen bonds with $His^{345}$, $Pro^{346}$, $His^{505}$, and $Arg^{518}$. **L4** and **L5** each form a single H-bond with $His^{345}$ (1.79 Å and 1.73 Å, respectively).

## Molecular Dynamics Simulation

In the current study, molecular dynamics MD simulations were used to investigate the stability of the **L2**/ACE2 complex over 100 ns using RMS deviation, RMS fluctuation, and protein-ligand H-bonds contact analysis, in addition to the radius of gyration (Rg), as shown in Table 6 and Fig. 10 (a to d).

The difference between two structures, a target and a reference structure, is estimated numerically as RMSD. In molecular dynamics, we focus on how structures and their component elements alter over time in relation to their initial position. A plot of RMSD vs time will show that a protein, throughout the course of a simulation, has a lid opening and shutting action. RMSD may be used to identify significant alterations in protein structure with respect to the starting point. One indication that the protein has stabilized is if the corresponding curve flattens or levels out. The RMSD of **L2**/ACE2 complex showed no conformational changes and found a little shaky throughout 100 ns MD simulation with the value from 0-0.5762 nm (Table 6) with an average of 0.3886 nm; During the simulation, the **L2**/ACE2 complex initially deviated from 0 to 45 ns, then it stabilized with a RMSD value of 0.4 nm (indicated in orange in Fig. 10a), the RMSD values of the protein had the same trend as the complex. On the other hand, RMSD values for the **L2** ligand were found as 0-1.261 Å (indicated in blue in Fig. 10a).

Root mean square fluctuation is referred to as RMSF. This numerical measurement is comparable to RMSD, but instead of calculating position differences between entire structures over time, RMSF estimates a residue's flexibility, or how much it varies or moves, over the course of a simulation. When plotted against the number of residues, RMSF per residue can reveal which amino acids in a protein structurally contribute the most to molecular motion. In our molecular dynamics study, to identify the complex's local conformational changes and structural fluctuation, RMSF analysis of **L2**/ACE2 was performed. The RMSF plot is shown in Fig. 10b. It was observed that the maximum and minimum RMSF values are found to be 0.0568 and 0.6418 nm (Table 6), respectively. The fluctuation was associated particularly with the residues $Glu^{150}$, $Ala^{153}$, $Asn^{154}$, $Ser^{155}$, $Leu^{156}$, $Gly^{337}$, $Asn^{338}$ and $Asn^{397}$, which are not associated with the residues of the active site.

A set of atoms' radial distance from their axis of rotation is known as the radius of gyration (Rg). Rg values enable the evaluation of ligand conformational changes in relation to protein-binding sites. It therefore predicts how compactly a folded protein will be structurally. The Rg values related to the **L2**/ACE2 complex were found to range from 2.407 to 2.611 nm, as shown in Table 6. The Rg values (Fig. 10c) stabilized and compact, and a well-folded structure of the complex was conserved after 35 ns, H-bond interactions were used to examine the protein-ligand complexes' binding capacity (Fig. 10c). There are from 0 to 5 hydrogen bonds observed in the **L2**/1R4L complex, but during most of the simulation time, the ligand-protein had no hydrogen bond, which presents a certain instability of the **L2**/1R4L complex. SASA calculates the surface zone during the interaction of a ligand with the water molecule. Its values range between 242.393 and 300.026 $nm^2$ as shown in Table 6.

Regarding the RMSD, RMSF and Rg, the **L2**/1R4L complex could be considered relatively stable [96][97] despite the lack of hydrogen bonds in some periods during the 100 ns molecular dynamics simulation.

**Table 6.** RMSD, RMSF, Rg and SASA Values from MD Results

| | Min | Max | Average |
|---|---|---|---|
| RMSD Complex (nm) | 0 | 0.5762 | 0.3886 |
| RMSD Protein (nm) | 0 | 0.5438 | 0.3466 |
| RMSD Ligand L2 (nm) | 0 | 0.1261 | 0.0662 |
| RMSF (nm) | 0.0568 | 0.6418 | 0.159 |
| Radius of Gyration Rg (nm) | 2.4066 | 2.6105 | 2.5422 |
| SASA ($nm^2$) | 242.393 | 300.026 | 283.9091 |

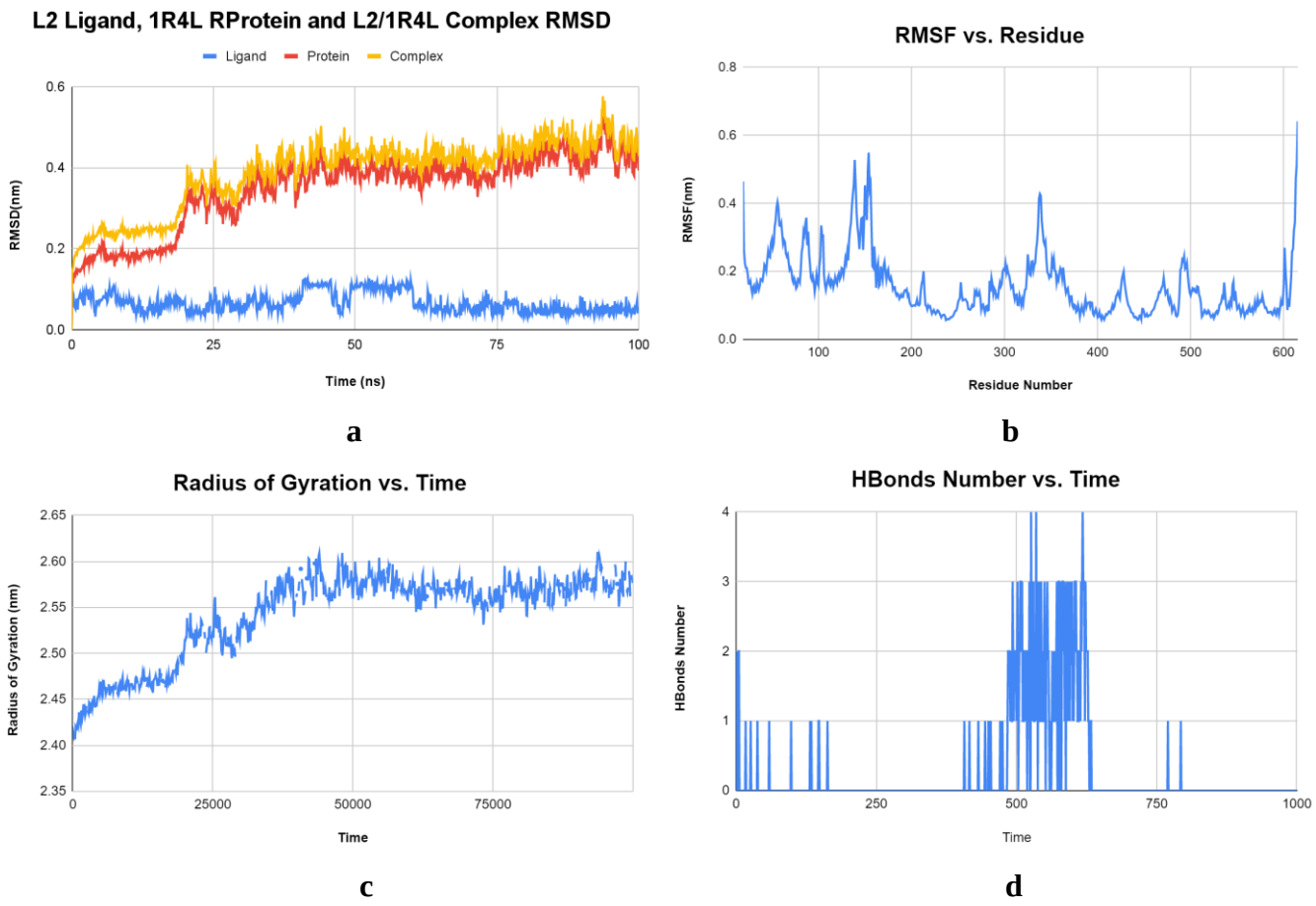


**Fig. 10.** MD simulation Results during 100 ns: (a) RMSD trajectories values *vs*. 100 ns, (b) RMSF trajectories values *vs*. Residue index, (c) Rg trajectories values *vs*. $10^5$ ps, (d) The number of hydrogen bonds (Hbond) *vs*. $1000*10^{-1}$ ns.

## Pharmacokinetics and Physicochemical Properties

To be as effective as a medicinal drug, the candidate molecule must reach the target enzyme inside the body at a sufficient dose and remain bioactive during the expected biological activities. Before going to the *in-vivo* test, it is necessary to assess the absorption, distribution, metabolism, excretion and toxicity (ADME-Tox) early [98]. To this end, the pkCSM webserver [67] was used as an alternative for the experiment to predict the ADME-Tox properties.

**Absorption.** The finding shown in Table 7 revealed that all test flavonoids had high absorption rates between 91% and 96%. According to the Norender team [99], the most effective compounds to cross the intestinal mucosal barrier are those with at least 30% absorption. It proves our compounds can be absorbed at the human intestinal level. In contrast, the reference compound MLN-4760 exhibited 41% absorption, which is close to the accepted lower limit.

**Distribution.** The blood-brain barrier (BBB) acts as a selectively permeable barrier between blood vessels and brain tissue cells. The BBB prevents pathogens and toxins present in the blood from penetrating the brain [100]. The logBB (or BBB permeability) is a parameter used to quantify the extent of drug penetration across the blood-brain barrier. The data in Table 7 indicate that blood-brain barrier permeability values for all compounds were in the low range of -1.671 to -0.224, which means that they do not reach the brain [101]. Besides, the central nervous system (CNS) permeability (or logPS) is an essential parameter for compounds targeting the CNS. From Table 7, all test compounds showed very low CNS penetrability values (from -3.362 to -2.176), reflecting the difficulty of moving through the CNS. It is also noted that the ligand **L2** value (CNS permeability -3.362) was lower than that recorded for all other ligands, including the reference one (MLN-4760).

Consequently, it will reduce undesirable effects, demonstrating its effectiveness and drug-like action [102].

**Metabolism.** Drug metabolism depends on CYP enzymes [103]. Several CYP isoforms, like 3A4 and 2D6, control the rate of drug biotransformation and how long they remain in the body. The excessive activity of these enzymes can render the drug ineffective. In contrast, if they are not active enough, the drug will remain in the body for a long time, which may lead to poisoning. Inhibition of cytochrome isoforms will undoubtedly make them less active, leading to unwanted effects due to lower drug clearance from the body. Results obtained in Table 7 show that all test ligands are non-inhibitors and non-substrates of the two main isoforms, 3A4 and 2D6, except the ligands **L1** and **L5**, which are inhibitors of CYP3A4 [103].

**Excretion and toxicity.** Concerning excretion, the clearance index recorded low values, which increases the stability of drugs in the body. Moreover, it is essential to examine our compounds early because drug selection is highly dependent on the extent of the compounds' expected toxicity [104]. Fortunately, the AMES toxicity, hepatotoxicity, and skin sensitisation tests proved that all test flavonoids are non-toxic, except for ligand **L1**, which is considered toxic in terms of AMES toxicity. In parallel, the reference molecule MLN-4760 has proven harmful in hepatotoxicity tests.

**Lipinski's rule.** The therapeutic potential of a drug candidate is highly related to its physicochemical properties. These properties are responsible for the biological activity of the molecule in the protein's active site. Table 7 summarizes some physicochemical properties for our test flavonoid compounds (**L1** to **L5**). These parameters were calculated by applying the SwissADME webserver [68] to each test molecule. According to Lipinski's rule of five, a candidate molecule must meet five threshold parameters to be considered a bioactive drug; molecular weight (MW) not more than 500 Daltons, lipophilicity ($logP_{o/w}$) ranging between -3 and 4, hydrogen bond acceptors (HBA) below 10, hydrogen bond donors (HBD) under than 5 and molar refractivity (MR) from 40 to 130 [105]. As shown in Table 7, the test flavonoids used in this investigation were consistent with Lipinski's rule.

**Table 7.** Predicted Physicochemical and ADME-Tox Properties

| Properties | | Predicted values | | | | | |
|---|---|---|---|---|---|---|---|
| | | **MLN-4760** | **L1** | **L2** | **L3** | **L4** | **L5** |
| Physicochemical properties | Lipinski's rule | | | | | | |
| MW (g $mol^{-1}$) | 500 ≤ | 428.31 | 314.29 | 330.29 | 314.29 | 254.29 | 270.24 |
| LogP | ≥ -3 and 4 ≤ | 1.91 | 2.47 | 2.1 | 2.52 | 2.55 | 2.11 |
| HBA | 10 ≤ | 6 | 6 | 7 | 6 | 4 | 5 |
| HBD | 05 < | 3 | 2 | 3 | 2 | 2 | 3 |
| MR | ≥ 40 and 130 ≤ | 104.76 | 84.95 | 86.97 | 84.95 | 71.97 | 73.99 |
| Absorption | | | | | | | |
| Intestinal absorption (human) | Numeric (% Abs) | 41.224 | 96.016 | 95.389 | 95.802 | 95.802 | 91.502 |
| Distribution | | | | | | | |
| BBB permeability | Numeric (log BB) | -1.671 | -0.224 | -1.351 | -0.253 | -0.253 | -0.957 |
| CNS permeability | Numeric (log PS) | -2.996 | -2.392 | -3.362 | -2.379 | -2.379 | -2.176 |
| Metabolism | | | | | | | |
| CYP-2D6 substrate | Categorical (Yes/No) | No | No | No | No | No | No |
| CYP-3A4 substrate | Categorical (Yes/No) | No | No | No | No | No | No |
| CYP-2D6 inhibitor | Categorical (Yes/No) | No | No | No | No | No | No |
| CYP-3A4 inhibitor | Categorical (Yes/No) | No | Yes | No | No | No | Yes |
| Excretion | | | | | | | |
| Total clearance | (log ml/min/kg) | 0.134 | 0.773 | 0.689 | 0.762 | 0.762 | 0.693 |
| Renal OCT2 substrate | Categorical (Yes/No) | No | No | No | No | No | No |
| Toxicity | | | | | | | |
| AMES toxicity | Categorical (Yes/No) | No | Yes | No | No | No | No |
| Hepatotoxicity | Categorical (Yes/No) | Yes | No | No | No | No | No |
| Skin sensitisation | Categorical (Yes/No) | No | No | No | No | No | No |

## CONCLUSIONS

This study evaluated five flavonoids from Algerian propolis as dual-function agents with antioxidant and ACE2 inhibitory potential using computational approaches. All compounds exhibited favorable antiradical behavior and stable interactions with ACE2, with energy scores ranging from -6.31 to -9.67 kcal $mol^{-1}$. Among them, pilosin (**L2**) demonstrated the highest radical scavenging capacity (attributed to its 8-OH group) and the most favorable interactions with ACE2, including binding to key residues and the zinc ion. Molecular dynamics simulations confirmed the stability of the pilosin/ACE2 complex over 100 ns. Notably, the 8-OH group may contribute to a synergic effect that enhances its interaction with the ACE2 active site. ADMET predictions indicated good oral bioavailability for all compounds, except **L1**, which was toxic in the AMES. These findings highlight pilosin as a promising drug-like candidate with combined antioxidant and antiviral properties. Future in vitro and in vivo validation studies are required to confirm its therapeutic potential and safety.

## ACKNOWLEDGMENT

This work was supported by the General Directorate of Scientific Research and Technological Development (DGRSDT). The authors gratefully acknowledge the Algerian Ministry of Higher Education and Scientific Research (MESRS) for financial support through PRFU projects B00L01UN240120230002 and B00L01UN240120230005.

## REFERENCES

1. Huang, L. L.; Shen, S. P.; Yu, P.; Wei, Y. Y., Dynamic basic reproduction number–based evaluation for current prevention and control of COVID-19 outbreak in China. *Zhonghua Liu Xing Bing Xue Za Zhi* **2020**, *41*, 466-469, DOI: 10.3760/cma.j.cn112338-20200209-00080.
2. Medina-Enríquez, M. M., ACE2: the molecular doorway to SARS-CoV-2. *Cell Biosci.* **2020**, *10*, 1-17, DOI: 10.1186/s13578-020-00519-8.
3. Gamakaranage, C., Symptomatology of Coronavirus Disease 2019 (COVID-19): Lessons from a meta-analysis across 13 countries. **2020**.
4. Paderno, A.; Schreiber, A.; Grammatica, A.; *et al*., Smell and taste alterations in COVID-19: a cross-sectional analysis of different cohorts. *Int. Forum Allergy Rhinol.* **2020**, *10*, 955-962, DOI: 10.1002/alr.22610.
5. Mounadi, N.; Nour, H.; Errougui, A.; Talbi, M.; ElKouali, M.; Chtita, S., Discovery of eugenol-derived drug candidates for the treatment of COVID-19 by applying molecular docking, molecular dynamics, and pharmacokinetic analysis. *Phys. Chem. Res.* **2024**, *12* (2), 289-303, DOI: 10.22036/pcr.2023.409956.2390.
6. Xu, X.; Chen, P.; Wang, J.; *et al*., Evolution of the novel coronavirus from the ongoing Wuhan outbreak and modeling of its spike protein for risk of human transmission. *Sci. China Life Sci.* **2020**, *63*, 457-460, DOI: 10.1007/s11427-020-1637-5.
7. Lan, J.; Ge, J.; Yu, J.; *et al*., Structure of the SARS-CoV-2 spike receptor-binding domain bound to the ACE2 receptor. *Nature* **2020**, 581, 215-220, DOI: 10.1038/s41586-020-2180-5.
8. Soltani, M.; Sardari, S.; Sabzyan, H.; Ghasemi, F., Towards screening and repurposing of approved drugs for the treatment of COVID-19 using molecular docking. *Phys. Chem. Res.* **2023**, *11* (4), 707-723, DOI: 10.22036/pcr.2022.353920.2192.
9. Wang, Q.; Zhang, Y.; Wu, L.; *et al*., Structural and functional basis of SARS-CoV-2 entry by using human ACE2. *Cell* **2020**, *181*, 894-904.e9, DOI: 10.1016/j.cell.2020.03.045.
10. Wrapp, D.; Wang, N.; Corbett, K. S.; *et al*., Cryo-EM structure of the 2019-nCoV spike in the prefusion conformation. *Science* **2020**, *367*, 1260-1263, DOI: 10.1126/science.abb2507.
11. Abidi, M.; Soheilifard, R.; Ghasemi, R. H., Comparison of the unbinding process of RBD-ACE2 complex between SARS-CoV-2 variants (Delta, delta plus, and Lambda): A steered molecular dynamics simulation. *Mol. Simul.* **2022**, *48*, 1660-1667, DOI: 10.1080/08927022.2022.2114599.
12. Ahmad, I.; Pawara, R.; Surana, S.; Patel, H., The Repurposed ACE2 Inhibitors: SARS-CoV-2 Entry

Blockers of Covid-19. *Top. Curr. Chem.* **2021**, *379*, 40, DOI: 10.1007/s41061-021-00353-7.

13. Bardelčíková, A.; Miroššay, A.; Šoltýs, J.; Mojžiš, J., Therapeutic and prophylactic effect of flavonoids in post-COVID-19 therapy. *Phytother. Res.* **2022**, *36*, 2042-2060, DOI: 10.1002/ptr.7436.
14. Parihar, A.; Ahmed, S. S.; Sharma, P.; *et al*., Plant-based bioactive molecules for targeting of endoribonuclease using steered molecular dynamic simulation approach: a highly conserved therapeutic target against variants of SARS-CoV-2. *Mol. Simul.* **2022**, 1-13, DOI: 10.1080/08927022.2022.2113811.
15. Sangeetha, R.; Premkumar, R.; Maithili, S. S.; *et al*., Spectroscopic, solvent effect, molecular docking and molecular dynamics investigations on phytocompounds from Elettaria cardamomum against COVID-19. *Polycycl. Aromat. Compd.* **2022**, 1-19, DOI: 10.1080/10406638.2022.2086270.
16. Cowan, M. M., Plant products as antimicrobial agents. *Clin. Microbiol. Rev.* **1999**, *12*, 564-582, DOI: 10.1128/CMR.12.4.564.
17. Bakkali, F.; Averbeck, S.; Averbeck, D.; Idaomar, M., Biological effects of essential oils a review. *Food Chem. Toxicol.* **2008**, *46*, 446-475, DOI: 10.1016/j.fct.2007.09.106.
18. Saklani, A.; Kutty, S. K., Plant-derived compounds in clinical trials. *Drug Discov. Today* **2008**, *13*, 161-171, DOI: 10.1016/j.drudis.2007.10.010.
19. Berretta, A. A.; Silveira, M. A. D.; Cóndor Capcha, J. M.; De Jong, D., Propolis and its potential against SARS-CoV-2 infection mechanisms and COVID-19 disease. *Biomed. Pharmacother.* **2020**, *131*, 110622, DOI: 10.1016/j.biopha.2020.110622.
20. Maruta, H.; He, H., PAK1-blockers: Potential therapeutics against COVID-19. *Med. Drug Discov.* **2020**, *6*, 100039, DOI: 10.1016/j.medidd.2020.100039.
21. Zabaiou, N.; Fouache, A.; Trousson, A.; *et al*., Biological properties of propolis extracts: Something new from an ancient product. *Chem. Phys. Lipids* **2017**, *207*, 214-222, DOI: 10.1016/j.chemphyslip.2017.04.005.
22. Kujumgiev, A.; Tsvetkova, I.; Serkedjieva, Y.; *et al*., Antibacterial, antifungal and antiviral activity of propolis of different geographic origin. *J. Ethnopharmacol.* **1999**, *64*, 235-240, DOI: 10.1016/s0378-8741(98)00131-7.
23. Hachem, K.; Bokov, D.; Mahdavian, L., Antioxidant capacity of caffeic acid phenethyl ester in scavenging free radicals by a computational insight. *Polycycl. Aromat. Compd.* **2023**, *43*, 2770-2787, DOI: 10.1080/10406638.2022.2053174.
24. Campos, J. F.; Dos Santos, U. P.; da Rocha, P. D. S.; *et al.*, Antimicrobial, antioxidant, anti-inflammatory, and cytotoxic activities of propolis from the stingless bee Tetragonisca fiebrigi (Jataí). *Evid. Based Complement. Alternat. Med.* **2015**, 296186, DOI: 10.1155/2015/296186.
25. Búfalo, M. C.; Bordon-Graciani, A. P.; Conti, B. J.; *et al*., The immunomodulatory effect of propolis on receptors expression, cytokine production and fungicidal activity of human monocytes. *J. Pharm. Pharmacol.* **2014**, *66*, 1497-1504, DOI: 10.1111/jphp.12279.
26. Chan, G. C. -F.; Cheung, K. -W.; Sze, D. M. -Y., The immunomodulatory and anticancer properties of propolis. *Clin. Rev. Allergy Immunol.* **2013**, *44*, 262-273, DOI: 10.1007/s12016-012-8322-2.
27. Al-Ani, I.; Zimmermann, S.; Reichling, J.; Wink, M., Antimicrobial activities of European propolis collected from various geographic origins alone and in combination with antibiotics. *Medicines (Basel)* **2018**, *5*, 1-14, DOI: 10.3390/medicines5010002.
28. Ferreira, J. M.; Fernandes-Silva, C. C.; Salatino, A.; *et al*., New propolis type from north-east Brazil: chemical composition, antioxidant activity and botanical origin. *J. Sci. Food Agric.* **2017**, *97*, 3552-3558, DOI: 10.1002/ jsfa.8210.
29. Anjum, S. I.; Ullah, A.; Khan, K. A.; *et al*., Composition and functional properties of propolis (bee glue): A review. *Saudi J. Biol. Sci.* **2019**, *26*, 1695-1703, DOI: 10.1016/j.sjbs.2018.08.013.
30. Menacer, R.; Rekkab, S.; Kabouche, Z., Fisetin and Robinetin antiradical activity under solvent effect: density functional theory study. *J. Mol. Model.* **2022**, *28*, 240, DOI: 10.1007/s00894-022-05223-7.
31. Sendi, N.; Ben Mansour, R.; Selmi, S.; *et al*., Simultaneous optimization of ultrasound-assisted extraction of flavonoid compounds and antiradical activity from Artemisia herba-Alba using response

surface methodology. *Prep. Biochem. Biotechnol.* **2020**, 1-13, DOI: 10.1080/10826068.2020.1774778.

32. Yenil, N.; Yemiş, F.; Sabikoglu, İ.; *et al*., Comparative analyses of few west Turkish varieties of pomegranate (Punica granatum L.) peels for phenolic content using liquid chromatography. *Polycycl. Aromat. Compd.* **2022**, 1-17, DOI: 10.1080/10406638.2022.2080727.
33. Hussain, F.; Jahan, N.; Rahman, K. -U.; *et al*., Identification of hypotensive biofunctional compounds and evaluation of their angiotensin-converting enzyme (ACE) inhibition potential. *Oxid. Med. Cell Longev.* **2018**, 4643736, DOI: 10.1155/2018/4643736.
34. Lubbe, L.; Cozier, G. E.; Oosthuizen, D.; *et al*., ACE2 and ACE: structure-based insights into mechanism, regulation and receptor recognition by SARS-CoV. *Clin. Sci.* **2020**, *134*, 2851-2871, DOI: 10.1042/CS20200899.
35. Mehra, M. R.; Desai, S. S.; Kuy, S.; *et al*., Cardiovascular disease, drug therapy, and mortality in Covid-19. *N. Engl. J. Med.* **2020**, *382*, e102, DOI: 10.1056/NEJMoa2007621.
36. Guler, H. I.; Tatar, G.; Yildiz, O.; *et al*., Investigation of potential inhibitor properties of ethanolic propolis extracts against ACE-II receptors for COVID-19 treatment by molecular docking study. *Arch. Microbiol.* **2021**, *203*, 3557-3564, DOI: 10.1007/s00203-021-02351-1.
37. Khayrani, A. C.; Irdiani, R.; Aditama, R.; *et al*., Evaluating the potency of Sulawesi propolis compounds as ACE-2 inhibitors through molecular docking for COVID-19 drug discovery preliminary study. *J. King Saud Univ. Sci.* **2021**, *33*, 101297, DOI: 10.1016/j.jksus.2020.101297.
38. Ghosh, S.; Al-Sharify, Z. T.; Maleka, M. F.; *et al*., Propolis efficacy on SARS-COV viruses: a review on antimicrobial activities and molecular simulations. *Environ. Sci. Pollut. Res. Int.* **2022**, *29*, 58628-58647, DOI: 10.1007/s11356-022-21652-6.
39. Segueni, N.; Akkal, S.; Benlabed, K.; Nieto, G., Potential use of propolis in phytocosmetic as phytotherapeutic constituent. *Molecules* **2022**, *27*, 1-18, DOI: 10.3390/molecules27185833.
40. Boulechfar, S.; Akbulut, Z.; Tepe, H. D.; *et al*., LC–MS/MS analysis, antioxidant and anticancer effects of phenolic-rich extracts from Algerian propolis: a comparative study. *J. Food Meas. Charact.* **2023**, *17*, 564-575, DOI: 10.1007/s11694-022-01652-3.
41. Boulechfar, S.; Zellagui, A.; Bensouici, C.; *et al*., Anticholinesterase, anti-α-glucosidase, antioxidant and antimicrobial effects of four Algerian propolis. *J. Food Meas. Charact.* **2022**, *16*, 793-803, DOI: 10.1007/s11694-021-01203-2.
42. Soltani, E. -K.; Cerezuela, R.; Charef, N.; *et al*., Algerian propolis extracts: Chemical composition, bactericidal activity and *in vitro* effects on gilthead seabream innate immune responses. *Fish Shellfish Immunol.* **2017**, *62*, 57-67, DOI: 10.1016/j.fsi.2017.01.009.
43. Segueni, N.; Zellagui, A.; Moussaoui, F.; *et al*., Flavonoids from Algerian propolis. *Arab J. Chem.* **2016**, *9*, S425-S428, DOI: 10.1016/j.arabjc.2011.05.013.
44. Frisch, M.; Trucks, G. W.; Schlegel, H. B.; *et al*., *Gaussian 09, Revision D.01*; Gaussian, Inc.: Wallingford, CT, **2009**.
45. Becke, A. D., Density-functional exchange-energy approximation with correct asymptotic behavior. *Phys. Rev. A* **1988**, *38*, 3098-3100, DOI: 10.1103/PhysRevA.38.3098.
46. Chahira, L.; El Faydyb, M.; Adlanic, L.; *et al*., Explanation of the quinoxaline analog's adsorption and inhibition mechanism for carbon steel corrosion in 1 M HCl based on experiments and theoretical calculations. *Phys. Chem. Res.* **2024**, *14*, 881-899, DOI: 10.22036/pcr.2024.440352.2472.
47. Nour, H.; Salhy, A.; Rossafi, B.; Mounadi, N.; Chtita, S., Identification of potent hepcidin antagonists for anemia treatment: In silico drug repositioning study. *Phys. Chem. Res.* **2025**, *13*, 429-442, DOI: 10.22036/pcr.2025.498178.2624.
48. Ram Kumara, A.; Senthamil Selvi, C.; Selvaraj, C.; Sheeja, M. G. P.; Jayaprakash, P., *In silico* studies on the molecular geometry, FMO, Mulliken charges, MESP, ADME and molecular docking prediction of pyrogallol carboxaldehydes as potential anti-tumour agents. *Phys. Chem. Res.* **2024**, *12*, 305-320, DOI: 10.22036/pcr.2023.402835.2359.
49. Boukilia, B.; Kaotar Hnawic, S.; Mennasb, I.; et al., TD-DFT screening of acrylic-based organic D-Π-A dye molecules for reliable and highly efficient dye-sensitized

solar cells. *Phys. Chem. Res.* **2025**, *13*, 545-556, DOI: 10.22036/pcr.2025.522084.2681.

50. Liu, Y.; Liu, C.; Li, J., Comparison of vitamin C and its derivative antioxidant activity: Evaluated by using density functional theory. *ACS Omega* **2020**, *5*, 25467-25475, DOI: 10.1021/acsomega.0c04318.
51. Rimarčík, J.; Lukeš, V.; Klein, E.; Ilčin, M., Study of the solvent effect on the enthalpies of homolytic and heterolytic N–H bond cleavage in p-phenylenediamine and tetracyano-p-phenylenediamine. *Theochem* **2010**, *952*, 25-30, DOI: 10.1016/j.theochem.2010.04.002.
52. Bizarro, M. M.; Cabral, B. J. C.; dos Santos, R. M. B.; Simões, J. A. M., Substituent effects on the O–H bond dissociation enthalpies in phenolic compounds: agreements and controversies + erratum. *Pure Appl. Chem.* **1999**, *71*, 1249-1256, DOI: 10.1351/pac199971071249.
53. Parker, V. D., Homolytic bond (H-A) dissociation free energies in solution. Applications of the standard potential of the (H+/H.bul.) couple. *J. Am. Chem. Soc.* **1992**, *114*, 7458-7462, DOI: 10.1021/ja00045a018.
54. Thong, N. M.; Quang, D. T.; Bui, N. H. T.; *et al*., Antioxidant properties of xanthones extracted from the pericarp of Garcinia mangostana (Mangosteen): A theoretical study. *Chem. Phys. Lett.* **2015**, *625*, 30-35, DOI: 10.1016/j.cplett.2015.02.033.
55. Towler, P.; Staker, B.; Prasad, S. G.; *et al*., ACE2 X-ray structures reveal a large hinge-bending motion important for inhibitor binding and catalysis. *J. Biol. Chem.* **2004**, *279*, 17996-18007, DOI: 10.1074/jbc.M311191200.
56. Biovia, D. S., *Discovery Studio Visualizer*; San Diego, CA, USA, **2017**.
57. Morris, G. M.; Huey, R.; Lindstrom, W.; *et al*., AutoDock4 and AutoDockTools4: Automated docking with selective receptor flexibility. *J. Comput. Chem.* **2009**, *30*, 2785-2791, DOI: 10.1002/jcc.21256.
58. Afriza, D.; Suriyah, W. H.; Ichwan, S. J. A., *In silico* analysis of molecular interactions between the anti-apoptotic protein survivin and dentatin, nordentatin, and quercetin. *J. Phys. Conf. Ser.* **2018**, *1073*, 032001, DOI: 10.1088/1742-6596/1073/3/032001.
59. Aimene, Y.; Eychenne, R.; Rodriguez, F.; *et al*., Synthesis, crystal structure, inhibitory activity and molecular docking of coumarins/sulfonamides containing triazolyl pyridine moiety as potent selective Carbonic Anhydrase IX and XII inhibitors. *Crystals (Basel)* **2021**, *11*, 1076, DOI: 10.3390/cryst11091076.
60. Pagadala, N. S.; Syed, K.; Tuszynski, J., Software for molecular docking: a review. *Biophys. Rev.* **2017**, *9*, 91-*102*, DOI: 10.1007/s12551-016-0247-1.
61. Fine, J.; Konc, J.; Samudrala, R.; Chopra, G., CANDOCK: Chemical atomic network-based hierarchical flexible docking algorithm using generalized statistical potentials. *J. Chem. Inf. Model.* **2020**, *60*, 1509-1527, DOI: 10.1021/acs.jcim.9b00686.
62. Ramírez, D.; Caballero, J., Is it reliable to take the molecular docking top scoring position as the best solution without considering available structural data? *Molecules* **2018**, *23*, 510, DOI: 10.3390/molecules23051038.
63. Jo, S.; Kim, T.; Iyer, V. G.; Im, W., CHARMM-GUI: A web-based graphical user interface for CHARMM. *J. Comput. Chem.* **2008**, *29*, 1859-1865, DOI: 10.1002/jcc.20945.
64. Lee, J.; Cheng, X.; Swails, J. M.; *et al*., CHARMM-GUI input generator for NAMD, GROMACS, AMBER, OpenMM, and CHARMM/OpenMM simulations using the CHARMM36 additive force field. *J. Chem. Theory Comput.* **2016**, *12*, 405-413, DOI: 10.1021/acs.jctc.5b00935.
65. Abraham, M. J.; Murtola, T.; Schulz, R.; *et al*., GROMACS: High performance molecular simulations through multi-level parallelism from laptops to supercomputers. *SoftwareX* **2015**, *1-2*, 19-25, DOI: 10.1016/j.softx.2015.06.001.
66. Humphrey, W.; Dalke, A.; Schulten, K., VMD: Visual molecular dynamics. *J. Mol. Graph.* **1996**, *14*, 33-38, 27-28, DOI: 10.1016/0263-7855(96)00018-5.
67. Pires, D. E. V.; Blundell, T. L.; Ascher, D. B., pkCSM: Predicting small-molecule pharmacokinetic and toxicity properties using graph-based signatures. *J. Med. Chem.* **2015**, 58, 4066-4072, DOI: 10.1021/acs.jmedchem.5b00104.
68. Daina, A.; Michielin, O.; Zoete, V., SwissADME: A free web tool to evaluate pharmacokinetics, drug-likeness and medicinal chemistry friendliness of small molecules. *Sci. Rep.* **2017**, *7*, 42717, DOI: 10.1038/srep42717.

69. Li, M.; Liu, W.; Peng, C.; *et al*., A DFT study on reaction of eupatilin with hydroxyl radical in solution. *Int. J. Quantum Chem.* **2013**, *113*, 966-974, DOI: 10.1002/qua.24060.
70. Pérez-González, A.; Galano, A., On the •OH and •OOH scavenging activity of 3-methyl-1-pyridin-2-yl-5-pyrazolone: Comparisons with its parent compound, edaravone. *Int. J. Quantum Chem.* **2012**, *112*, 3441-3448, DOI: 10.1002/qua.24046.
71. Pérez-González, A.; Galano, A., OH radical scavenging activity of edaravone: Mechanism and kinetics. *J. Phys. Chem. B* **2011**, *115*, 1306-1314, DOI: 10.1021/jp110400t.
72. Seridi, S.; Dinar, K.; Seridi, A.; *et al*., Charge transfer complexes of 4-isopropyl-2-benzyl-1,2,5-thiadiazolidin-3-one 1,1-dioxide with DDQ and TCNE: Experimental and DFT studies. *New J. Chem.* **2016**, *40*, 4781-4792, DOI: 10.1039/c5nj03017j.
73. Prasad, O.; Sinha, L.; Misra, N.; *et al*., Molecular structure and vibrational study on 2,3-dihydro-1H-indene and its derivative 1H-indene-1,3(2H)-dione by density functional theory calculations. *Theochem* **2010**, *940*, 82-86, DOI: 10.1016/j.theochem.2009.10.011.
74. Janak, J. F., Proof that $\partial E/\partial n_i = \varepsilon_i$ in density-functional theory. *Phys. Rev. B* **1978**, *18*, 7165-7168, DOI: 10.1103/PhysRevB.18.7165.
75. Mendoza-Wilson, A. M.; Glossman-Mitnik, D., CHIH-DFT study of the electronic properties and chemical reactivity of quercetin. *Theochem* **2005**, *716*, 67-72, DOI: 10.1016/j.theochem.2004.10.083.
76. Chattaraj, P. K.; Roy, D. R., Update 1 of: Electrophilicity index. *Chem. Rev.* **2007**, *107*, PR46-PR74, DOI: 10.1021/cr078014b.
77. Zhan, C. -G.; Nichols, J. A.; Dixon, D. A., Ionization potential, electron affinity, electronegativity, hardness, and electron excitation energy: Molecular properties from density functional theory orbital energies. *J. Phys. Chem. A* **2003**, *107*, 4184-4195, DOI: 10.1021/jp0225774.
78. Parr, R. G.; Pearson, R. G., Absolute hardness: Companion parameter to absolute electronegativity. *J. Am. Chem. Soc.* **1983**, *105*, 7512-7516, DOI: 10.1021/ja00364a005.
79. Parr, R. G.; Szentpály, L. V.; Liu, S., Electrophilicity index. *J. Am. Chem. Soc.* **1999**, *121*, 1922-1924, DOI: 10.1021/ja983494x.
80. Ajmala Shireen, P.; Muraleedharan, K.; Abdul Mujeeb, V. M., Theoretical studies on anti-oxidant potential of alpinetin. *Mater. Today* **2018**, *5*, 8908-8915, DOI: 10.1016/j.matpr.2017.12.325.
81. Parr, R. G., Density functional theory of atoms and molecules. In *Horizons of Quantum Chemistry*; Springer Netherlands: Dordrecht, **1980**, pp. 5-15.
82. Fuhrmann, J.; Rurainski, A.; Lenhof, H. -P.; Neumann, D., A new Lamarckian genetic algorithm for flexible ligand-receptor docking. *J. Comput. Chem.* **2010**, *31*, 1911-1918, DOI: 10.1002/jcc.21478.
83. Du, X.; Li, Y.; Xia, Y. -L.; *et al*., Insights into protein-ligand interactions: Mechanisms, models, and methods. *Int. J. Mol. Sci.* **2016**, *17*, 201, DOI: 10.3390/ijms17020144.
84. Kitchen, D. B.; Decornez, H.; Furr, J. R.; Bajorath, J., Docking and scoring in virtual screening for drug discovery: Methods and applications. *Nat. Rev. Drug Discov.* **2004**, *3*, 935-949, DOI: 10.1038/nrd1549.
85. Ferrara, P.; Gohlke, H.; Price, D. J.; *et al*., Assessing scoring functions for protein-ligand interactions. *J. Med. Chem.* **2004**, *47*, 3032-3047, DOI: 10.1021/jm030489h.
86. Teralı, K.; Baddal, B.; Gülcan, H. O., Prioritizing potential ACE2 inhibitors in the COVID-19 pandemic: Insights from a molecular mechanics-assisted structure-based virtual screening experiment. *J. Mol. Graph. Model.* **2020**, *100*, 107697, DOI: 10.1016/j.jmgm.2020.107697.
87. Kawai, K.; Nagata, N., Metal-ligand interactions: An analysis of zinc binding groups using the Protein Data Bank. *Eur. J. Med. Chem.* **2012**, *51*, 271-276, DOI: 10.1016/j.ejmech.2012.02.028.
88. Aimene, Y.; Eychenne, R.; Mallet-Ladeira, S.; *et al*., Novel Re(I) tricarbonyl coordination compounds based on 2-pyridyl-1,2,3-triazole derivatives bearing a 4-amino-substituted benzenesulfonamide arm: Synthesis, crystal structure, computational studies and inhibitory activity against carbonic anhydrase I, II, and IX isoforms. *J. Enzyme Inhib. Med. Chem.* **2019**, *34*, 773-782, DOI: 10.1080/14756366.2019.1585835.

89. Arora, R.; Tchertanov, L., *The HIV-1 integrase: Modeling and beyond*. In An Integrated View of the Molecular Recognition and Toxinology - From Analytical Procedures to Biomedical Applications; InTech, **2013**.
90. Guy, J. L.; Jackson, R. M.; Jensen, H. A.; *et al*., Identification of critical active-site residues in angiotensin-converting enzyme-2 (ACE2) by site-directed mutagenesis. *FEBS J.* **2005**, *272*, 3512-3520, DOI: 10.1111/j.1742-4658.2005.04756.x.
91. Khan, S.; Ullah, H.; Taha, M.; *et al*., Synthesis, DFT studies, molecular docking and biological activity evaluation of thiazole-sulfonamide derivatives as potent Alzheimer's inhibitors. *Molecules* **2023**, *28*, 559.
92. Malak, N.; Alotaibi, B. S.; Khan, A.; *et al*., Density functional theory calculations and molecular docking analyses of flavonoids for their possible application against the acetylcholinesterase and triose-phosphate isomerase proteins of Rhipicephalus microplus. *Molecules* **2023**, *28*, 3606.
93. Kamel, E. M.; Bin-Ammar, A.; El-Bassuony, A.; *et al*., Molecular modeling and DFT studies on the antioxidant activity of Centaurea scoparia flavonoids and molecular dynamics simulation of their interaction with β-lactoglobulin. *RSC Adv.* **2023**, *13*, 12361-12374.
94. Dey, D.; Paul, P. K.; Al Azad, S.; *et al.*, Molecular optimization, docking, and dynamic simulation profiling of selective aromatic phytochemical ligands in blocking the SARS-CoV-2 S protein attachment to ACE2 receptor: An *in-silico* approach of targeted drug designing. *J. Adv. Vet. Anim. Res.* **2021**, *8*, 24.
95. Obakachi, V. A.; Nchiozem-Ngnitedem, V. A.; Govender, K.; Govender, P., *In silico* exploration of natural xanthone derivatives as potential inhibitors of severe acute respiratory syndrome coronavirus 2 (SARS-CoV-2) replication and cellular entry. *J. Comput.-Aided Mol. Des.* **2025**, *39*, 7.
96. Zhang, Z. -B.; Xia, Y. -L.; Shen, J. -X.; *et al.*, Mechanistic origin of different binding affinities of SARS-CoV and SARS-CoV-2 spike RBDs to human ACE2. *Cells* **2022**, *11*, 1274, DOI: 10.3390/cells11081274.
97. Pirolli, D.; Righino, B.; Camponeschi, C.; *et al*., Repositioning of drugs against SARS-CoV-2 variants: A virtual screening approach combined with molecular dynamics simulations to target Spike Protein/ACE2 interface. **2022**.
98. Guler, H. I.; Ay, F. S.; Can, Z.; *et al*., Targeting CoV-2 Spike RBD and ACE-2 interaction with flavonoids of Anatolian propolis by in silico and *in vitro* studies in terms of possible COVID-19 therapeutics. *bioRxiv* **2021**.
99. Norinder, U.; Bergström, C. A. S., Prediction of ADMET properties. *ChemMedChem* **2006**, *1*, 920-937, DOI: 10.1002/cmdc.200600155.
100. Clark, D. E., *In silico* prediction of blood-brain barrier permeation. *Drug Discov. Today* **2003**, *8*, 927-933, DOI: 10.1016/s1359-6446(03)02827-7.
101. Nisha, C. M.; Kumar, A.; Vimal, A.; *et al*., Docking and ADMET prediction of few GSK-3 inhibitors divulges 6-bromoindirubin-3-oxime as a potential inhibitor. *J. Mol. Graph. Model.* **2016**, *65*, 100-107, DOI: 10.1016/j.jmgm.2016.03.001.
102. Abdelrheem, D. A.; Rahman, A. A.; Elsayed, K. N. M.; *et al*., Isolation, characterization, *in vitro* anticancer activity, DFT calculations, molecular docking, bioactivity score, drug-likeness and ADMET studies of eight phytoconstituents from brown alga Sargassum platycarpum. *J. Mol. Struct.* **2021**, *1225*, 129245, DOI: 10.1016/j.molstruc.2020.129245.
103. Šrejber, M.; Navrátilová, V.; Paloncýová, M.; *et al*., Membrane-attached mammalian cytochromes P450: An overview of the membrane's effects on structure, drug binding, and interactions with redox partners. *J. Inorg. Biochem.* **2018**, *183*, 117-136, DOI: 10.1016/j.jinorgbio.2018.03.002.
104. Hadni, H.; Elhallaoui, M., 3D-QSAR, docking and ADMET properties of aurone analogues as antimalarial agents. *Heliyon* **2020**, *6*, e03580, DOI: 10.1016/j.heliyon.2020.e03580.
105. Lipinski, C. A., Lead- and drug-like compounds: The rule-of-five revolution. *Drug Discov. Today Technol.* **2004**, *1*, 337-341, DOI: 10.1016/j.ddtec.2004.11.007.